

# The coevolution of the velocity and mass functions of galaxies and dark haloes

Kyu-Hyun Chae<sup>1,2\*</sup>

<sup>1</sup> Sejong University, Department of Astronomy and Space Science, 98 Gunja-dong, Gwangjin-Gu, Seoul 143-747, Republic of Korea

<sup>2</sup> Theoretical Astrophysics, Fermi National Accelerator Laboratory, P. O. Box 500, Batavia, IL 60510, USA

\* chae@sejong.ac.kr: On sabbatical leave at Fermilab

Accepted ..... Received .....; in original form .....

## ABSTRACT

We employ a bias-corrected abundance matching technique to investigate the coevolution of the  $\Lambda$ CDM dark halo mass function (HMF), the observationally derived velocity dispersion and stellar mass functions (VDF, SMF) of galaxies between  $z = 1$  and 0. We use for the first time the evolution of the VDF constrained through strong lensing statistics by Chae (2010) for galaxy-halo abundance matching studies. As a local benchmark we use a couple of  $z \sim 0$  VDFs (a Monte-Carlo realised VDF based on SDSS DR5 and a directly measured VDF based on SDSS DR6). We then focus on connecting the VDF evolution to the HMF evolution predicted by  $N$ -body simulations and the SMF evolution constrained by galaxy surveys. On the VDF-HMF connection, we find that the local dark halo virial mass-central stellar velocity dispersion ( $M_{\text{vir}}\sigma$ ) relation is in good agreement with the individual properties of well-studied low-redshift dark haloes, and the VDF evolution closely parallels the HMF evolution meaning little evolution in the  $M_{\text{vir}}\sigma$  relation. On the VDF-SMF connection, it is also likely that the stellar mass-stellar velocity dispersion ( $M_{\star}\sigma$ ) relation evolves little taking the abundance matching results together with other independent observational results and hydrodynamic simulation results. Our results support the simple picture that as the halo grows hierarchically, the stellar mass and the central stellar velocity dispersion grow in parallel. We discuss possible implications of this parallel coevolution for galaxy formation and evolution under the  $\Lambda$ CDM paradigm.

**Key words:** galaxies: evolution – galaxies: formation – galaxies: haloes – galaxies: kinematics and dynamics – galaxies: statistics – galaxies: structure

## 1 INTRODUCTION

The current  $\Lambda$ CDM hierarchical structure formation theory predicts robustly the evolution of the dark halo mass<sup>1</sup> function (HMF) over cosmic time (e.g., Springel et al. 2005; Warren et al. 2006; Reed et al. 2007; Lukic et al. 2007; Tinker et al. 2008; Klypin et al. 2010). Because visible galaxies are believed to form and reside within the haloes under the  $\Lambda$ CDM paradigm, the statistical functions of galaxies, such as the luminosity function (LF), the stellar mass function (SMF), and the stellar velocity (dispersion) function (VF, VDF), are also expected to evolve. Connection of these statistical functions of galaxies with the theoretical HMF is not straightforward due to, and

mirrors, the complex processes of galaxy formation and evolution including star formations, supernovae explosions, AGN activities and galaxy merging. Some recent works in the literature are focused on the connection of the HMF with the broadly measured stellar mass function (SMF) of galaxies (e.g., Conroy & Wechsler 2009; Moster et al. 2009; Guo et al. 2009). Notice that the SMF as well as the LF have mainly to do with the star formation history of galaxies.

Galaxy formation in the halo has dynamical consequences as well. As stars are formed in the inner halo, the halo responds and the inner halo dark matter distribution is modified (e.g., Blumenthal et al. 1986; Gnedin et al. 2004; Rudd et al. 2008; Abadi et al. 2009; Tissera et al. 2010). Consequently, not only the total (i.e. dark plus stellar) mass distribution but also the dark matter distribution may become different from the pure dark matter distribution predicted by the  $\Lambda$ CDM. This dynamical aspect of galaxy formation is a crucial part of cosmological studies. Ultimately,

<sup>1</sup> Throughout this refers to the total mass within the virial radius of the halo. Accordingly, it includes the stellar mass once the galaxy is formed.

the theory of galaxy formation should predict successfully the dynamical evolution as well as the star formation history of galaxies. The statistical property of the dynamics of galaxies is encoded in the VDF of galaxies. The local total VDF is carefully reconstructed by Chae (2010) using SDSS DR5 galaxy counts and intrinsic correlations between luminosities and velocities of galaxies. More recently, Bernardi et al. (2010) estimates directly the local total VDF based on SDSS DR6 measurements (of a DR4 sample). Chae (2010) then constrains the evolution of the VDF up to  $z \sim 1$  through the statistical properties of strong lensing galaxies based on the empirical result that the average total (luminous plus dark) mass profile of galaxies is isothermal in the optical region. Chae (2010) notices that the *differential* evolution of the derived VDF is qualitatively similar to the evolution of the theoretical HMF under the current  $\Lambda$ CDM paradigm.

In this work we make a detailed quantitative comparison between the VDF evolution constrained from strong lensing statistics through the method of Chae (2010) and the evolutions of mass functions (i.e. the HMF and the SMF) from the literature. In doing so, we investigate the local (statistical) correlations of the velocity dispersion ( $\sigma$ ) of a galaxy with the virial mass ( $M_{\text{vir}}$ ) of the surrounding halo and the stellar mass ( $M_*$ ) of the galaxy, i.e.  $\sigma(M_{\text{vir}})$  and  $\sigma(M_*)$ , and their evolutions out to  $z \sim 1$ . These empirical correlations will provide independent *statistical* constraints on the structures of galaxies and haloes and their evolutions. We investigate the implications of the local correlations for the baryon-modified dark halo structures in a following work. In this work we focus on the evolutions of the correlations. We find that the halo mass, the stellar mass and the stellar velocity dispersion are coevolving in a parallel way for  $0 \lesssim z \lesssim 1$ . We discuss the implications of this result for galaxy formation and evolution under the  $\Lambda$ CDM paradigm.

This paper is organised as follows. In 2, we describe the method of analysis and the statistical functions to be used in this work; some details of the analysis are given in the Appendix A. In §3, we investigate the connection between the (evolving) VDF of galaxies from the SDSS and strong lensing statistics and the HMF from N-body simulations. We obtain the relation  $\sigma(M_{\text{vir}})$  and its evolution. We also examine the compatibility of the evolutions of the VDF and the HMF. In §4, we compare the VDF evolution with the SMF evolution from galaxy surveys. We investigate the evolution of  $\sigma(M_*)$  and the compatibility of the current observationally constrained VDF and SMF. In §5, we discuss the implications of the results for galaxy formation and evolution in the context of the current  $\Lambda$ CDM structure formation paradigm and cosmological observations. We conclude in §6. Unless specified otherwise, we assume a WMAP 5 year  $\Lambda$ CDM cosmology (Dunkley et al. 2009) with  $(\Omega_{\text{m}0}, \Omega_{\Lambda0}) = (0.25, 0.75)$  and  $H_0 = 100h \text{ km s}^{-1} \text{ Mpc}^{-1}$ . When parameter  $h$  does not appear explicitly,  $h = 0.7$  is assumed. In Appendix B we compare the results of this work with the nearly concurrent results by Dutton et al. (2010). Dutton et al. (2010) focus on the connection between the circular velocity in the optical region (at about the projected half-light radius)  $v_{\text{opt}}$  and that at the virial radius  $v_{\text{vir}}$ . While Dutton et al. (2010) use various estimates of the halo mass including satellite kinematics, weak lensing and abundance matching, their results are confined to  $z \sim 0$ . Another important difference between Dutton et al. (2010)

and this work is that Dutton et al. (2010) use observed stellar mass-velocity relations while this work uses the observationally derived velocity dispersion functions for abundance matching.

## 2 METHOD: ABUNDANCE MATCHING OF STATISTICAL FUNCTIONS

A statistical function of galaxies or haloes at a given epoch is defined by

$$\phi(x) = \left| \frac{dn(>x)}{dx} \right|, \quad (1)$$

where  $x$  is the variable under consideration (e.g.  $\sigma$ ,  $M_*$ ,  $M_{\text{vir}}$ ) and  $n(>x)$  is the integrated comoving number density down to  $x$ .

We use the abundance matching method (e.g. Kravtsov et al. 2004; Vale & Ostriker 2004; Conroy et al. 2006) to relate statistically one variable ( $x$ ) to another ( $y$ ). Namely, we have

$$y = y(x) \quad \text{or} \quad x = x(y) \quad \text{from} \quad n(>x) = n(>y). \quad (2)$$

The key assumption for equation (2) to be valid is that the two variables are monotonically increasing functions of each other. The accuracy of the median relation between  $x$  and  $y$  derived from the abundance matching method depends on the nature of the intrinsic scatter of the true relation (see Tasitsiomi et al. 2004; Behroozi et al. 2010). In Appendix A, a simulation is carried out to investigate the possible effect of the intrinsic scatter. It turns out that based on an observationally motivated intrinsic scatter the abundance matching method reproduces the overall behaviour of the intrinsic relation up to a maximum bias of  $\sim 0.08$  dex in most cases. We estimate and correct the biases in our abundance matching analyses.

This work is primarily concerned with connecting the stellar velocity dispersion of a galaxy ( $\sigma$ ) to the dark halo virial mass ( $M_{\text{vir}}$ ) and the galaxy stellar mass ( $M_*$ ). For the VDF at  $z = 0$  we use the results from Chae (2010) and Bernardi et al. (2010) (Fig. 1). Specifically, we use the ‘A0’ VDF of Chae (2010) that is a result from combining the early-type and the late-type VDFs based on SDSS DR5 data. The Bernardi et al. (2010) VDF is a *direct* fit to all-type galaxies based on SDSS DR6. Bernardi et al. (2010) give various fit results depending on the range of velocity dispersion and fit method. For this work we use the fit result for  $\sigma > 125 \text{ km s}^{-1}$  (taking into account measurement errors) because this work is primarily concerned with the evolution of massive galaxies. We then use strong lensing statistical analysis of Chae (2010) to constrain the evolution of the VDF up to  $z = 1$ . The results are shown in Fig. 1. The result for the Chae (2010) VDF is a reproduction while that for the Bernardi et al. (2010) VDF is a new result. Notice that for the Bernardi et al. (2010) VDF a modified Schechter function introduced by Sheth et al. (2003) is used while for the Chae (2010) VDF a correction term is included. The simplicity of the Bernardi et al. (2010) VDF allows all four parameters of the function to be varied and constrained by strong lensing data in contrast to the Chae (2010) VDF for which some parameters must be fixed (see §5.3 of Chae 2010).

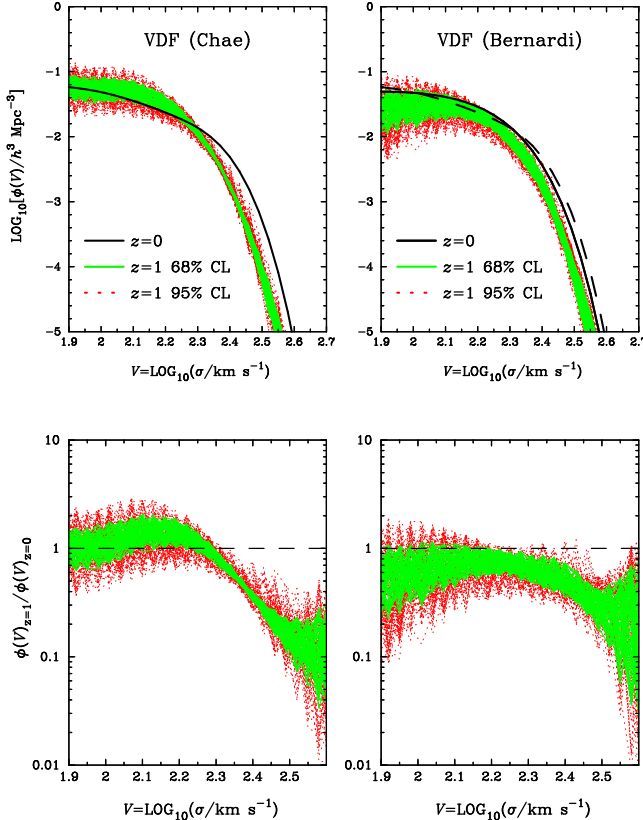


**Figure 1.** Velocity dispersion functions (VDFs) of galaxies at  $z = 0$  and  $z = 1$ . The VDFs at  $z = 0$  are those from Chae (2010) and Bernardi et al. (2010). The VDF by Chae (2010) is a sum of the early-type and late-type VDFs based on SDSS DR5 data. The VDF by Bernardi et al. (2010) is a direct fit for all galaxies based on SDSS DR6. The VDF by Chae (2010) is also reproduced as a dashed curve on the upper right panel for comparison. The constraints on the VDFs at  $z = 1$  are based on strong lensing statistics described in Chae (2010). Notice that strong lensing data probe only the range of  $95 \text{ km s}^{-1} \lesssim \sigma \lesssim 300 \text{ km s}^{-1}$  (see the texts in § 2).

Notice that the strong lensing surveys used to constrain the evolution of the VDF are limited to lensing galaxies with image splitting greater than 0.3 arcsec in the redshift range of  $0.3 \lesssim z \lesssim 1$  (see Chae 2010). This lower limit on image splitting implies that the constrained evolution of the VDF is strictly valid only for  $\sigma \gtrsim 95 \text{ km s}^{-1}$ . This in turn corresponds to  $M_\star \gtrsim 10^{10.2} M_\odot$  and  $M_{\text{vir}} \gtrsim 10^{11.6} M_\odot$  as will be shown below. Furthermore, although the surveys do not have physically meaningful upper limits on image separations, the surveys (because of the small sample sizes) have only identified lensing galaxies with measured or implied stellar velocity dispersion  $\sigma \lesssim 300 \text{ km s}^{-1}$  (with corresponding  $M_\star \lesssim 10^{11.8} M_\odot$  and  $M_{\text{vir}} \lesssim 10^{14.6} M_\odot$  as shown below). This is why the constraints on the VDF evolution become weak toward large  $\sigma$  as shown in Fig. 1. Hence any results from this work outside the above ranges must be regarded as extrapolations.

For the HMF we use a typical numerical result from N-body simulations under the current  $\Lambda$ CDM cosmology while for the SMF we use the results from some representative

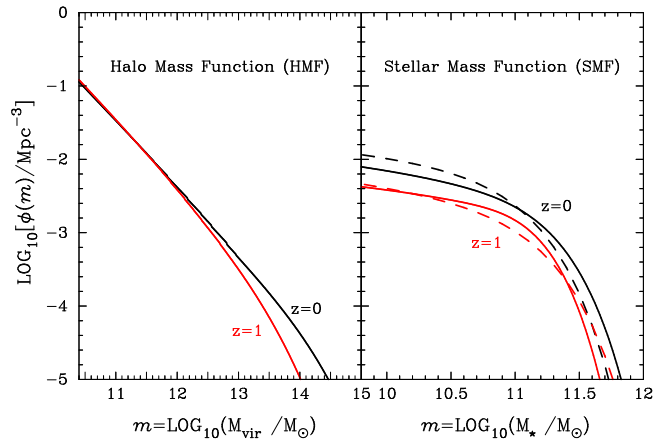


**Figure 2.** Left panel: A typical mass function for dark haloes as is produced from the  $\Lambda$ CDM simulation by Reed et al. (2007). The adopted cosmological parameters are  $(\Omega_{\text{m}0}, \Omega_{\Lambda0}) = (0.25, 0.75)$  and  $\sigma_8 = 0.8$ . The displayed function has been corrected to include subhaloes (see the texts in Section 3). Right panel: Observed stellar mass functions. Solid curves are from the COSMOS survey by Ilbert et al. (2010) while dashed curves are from the Spitzer survey by Pérez-González et al. (2008). Notice that the Spitzer results show stellar-mass-downsizing evolution of the SMF while the COSMOS results do not.

galaxy surveys. The HMF and the SMF are shown in Fig. 2 and more details are respectively given in Sections 3 and 4.

### 3 CONNECTION BETWEEN THE OBSERVATIONAL VDF AND THE HMF FROM N-BODY SIMULATIONS

In the  $\Lambda$ CDM hierarchical structure formation picture the dark halo mass function (HMF) evolves over cosmic time as a consequence of hierarchical merging (e.g. White & Rees 1978; Lacey & Cole 1993). Accordingly, the statistical functions of galaxies such as the VDF and the SMF are also expected to evolve. However, baryon physics complicates the evolutions of the VDF and the SMF making it non-trivial to compare the evolutions of the HMF, the SMF, and the VDF one another. Conversely, careful analyses of the coevolution of the HMF, the SMF, and the VDF may reveal key insights into galaxy formation and evolution processes. Here we compare the evolution of the VDF described in Section 2 with the evolution of the HMF from cosmological N-body simulations. A comparison between the VDF and the SMF is given in the next section.

The HMF may be determined analytically (e.g. Press & Schechter 1974; Sheth & Tormen 1999, 2002) or through  $N$ -body simulations (e.g. Jenkins et al. 2001; Springel et al. 2005; Warren et al. 2006; Reed et al. 2007; Lukić et al. 2007; Tinker et al. 2008). Recent high resolution  $N$ -body simulations have determined the HMF reliably (e.g. Warren et al. 2006; Reed et al. 2007; Lukić et al. 2007; Tinker et al. 2008). For the HMF we generate a numerical function using the code provided by Reed et al. (2007) taking the following cosmological parameters:  $\Omega_{\text{m}0} = 0.25$ ,  $\Omega_{\Lambda0} = 0.75$  and  $\sigma_8 = 0.8$  consistent with the WMAP5

data (Dunkley et al. 2009). This function includes only distinct haloes that are not parts of larger haloes. We correct it to include subhaloes since they may also host galaxies.<sup>2</sup> We use the simulation results by Conroy et al. (2006) for the number fraction of subhaloes ( $f_{\text{sub}}$ ) as a function of maximum circular velocity. By relating the maximum circular velocity to the halo virial mass using the scaling given by Klypin et al. (2010), we find a varying fraction from  $f_{\text{sub}} \approx 0.25$  ( $\approx 0.18$ ) at  $M_{\text{vir}} \lesssim 10^{11} M_{\odot}$  (this mass scale corresponds to the Conroy et al. (2006) completeness limit) to  $\approx 0.08$  ( $\approx 0.08$ ) at  $M_{\text{vir}} \gtrsim 10^{13} M_{\odot}$  for  $z = 0$  ( $z = 1$ ). Notice that the mass of a distinct halo refers to the epoch under consideration while that of a subhalo is the mass at the time it accreted onto a larger halo.

The mass of a halo ( $M_{\text{vir}}$ ) may be linked to the stellar velocity dispersion ( $\sigma$ ) of the central galaxy for those haloes that host galaxies. If the halo did not host a galaxy in its centre, the central velocity dispersion (of dark matter particles) would be entirely due to the dark mass potential. In reality, the central galaxy contributes to the central gravitational potential with the degree of contribution varying from one system to another. The functional relation  $\sigma(M_{\text{vir}})$  will depend not only on the stellar mass distribution of the residing galaxy but also how the dark halo has been modified due to the baryonic physics of galaxy formation. Moreover, the stellar mass distribution itself is correlated with  $M_{\text{vir}}$  to some degree. Thus, we may use the abundance matching relation between  $M_{\text{vir}}$  and  $\sigma$  to gain new insights into the structure of the baryon-modified dark halo and the dynamical aspect of galaxy formation and evolution.

### 3.1 The $M_{\text{vir}}-\sigma$ relation at $z = 0$

Fig. 3 shows the abundance matching  $M_{\text{vir}}-\sigma$  relation at  $z = 0$ . It shows both the relations ignoring intrinsic scatters and those taking into account an intrinsic scatter distribution of  $V \equiv \log_{10}(\sigma / \text{km s}^{-1})$  as a function of  $M_{\text{vir}}$ . For the latter case the intrinsic scatter distribution is predicted by a bivariate distribution of  $\sigma$  and  $M_{\star}$  as a function of  $M_{\text{vir}}$  based on an observed scatter of  $\log_{10}(M_{\star})$  at fixed  $M_{\text{vir}}$  and an observed scatter distribution of  $V$  as a function of  $M_{\star}$ . The reader is referred to Appendix A for a brief description and a following work (in preparation) for further details.

The abundance matching relation is compared against the measured values of  $M_{\text{vir}}$  and  $\sigma$  for individual galaxies/clusters with  $z \lesssim 0.3$ . Although there are numerous galaxies/clusters for which either  $\sigma$  or  $M_{\text{vir}}$  is reported, only for relatively few systems both  $M_{\text{vir}}$  and  $\sigma$  have been measured reliably so far. First, we consider the best-studied Milky Way galaxy, for which recent measurements appear to be reasonably concordant (Klypin et al. 2002; Battaglia et al. 2005, 2006; Xue et al. 2008).<sup>3</sup> The data from Xue et al. (2008) are displayed in Fig. 3. Second, we display the results for 22 SLACS lensing galaxies at mean redshift of  $z \sim 0.2$  by Gavazzi et al. (2007). They combine

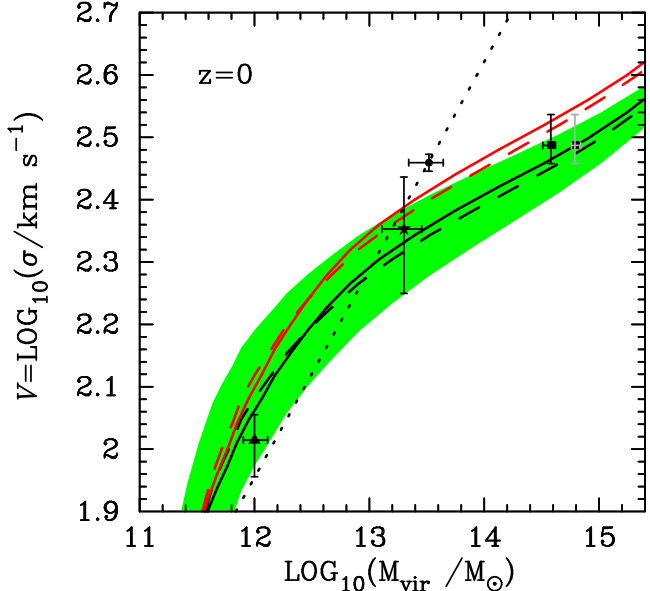


**Figure 3.** The relation between the halo virial mass ( $M_{\text{vir}}$ ) and the stellar velocity dispersion ( $\sigma$ ) of the central galaxy at  $z = 0$ , inferred from the abundance matching of the velocity dispersion function and the  $\Lambda$ CDM halo mass function (see the texts in §3). The red curves are the results ignoring the scatter of  $V \equiv \log_{10}(\sigma / \text{km s}^{-1})$  at fixed  $M_{\text{vir}}$ . The black curves are the results taking into account the scatter shaded green. See Appendix A for a brief description of the scatter. The solid and dashed curves are respectively based on the VDFs by Chae (2010) and Bernardi et al. (2010). The dotted line is a prediction of the SIS model of the halo. The curves are compared against the individual measurements for the following systems: *Triangles* - Milky Way (Xue et al. 2008). *Star* - A weighted mean of 22 SLACS lenses (Gavazzi et al. 2007) at  $z \sim 0.2$  taking the standard deviation of the individual mean values as the error on  $\sigma$ . *Circle* - Lens system Q0957+561 at  $z = 0.36$ . The velocity dispersion is from Tonry & Franx (1999) while the virial mass is from Nakajima et al. (2009). *Squares* - Galaxy cluster Abell 611 (Newman et al. 2009). The right square (gray) is based on the NFW halo model while the left square (solid) a generalised NFW halo model.

strong and weak lensing and stellar kinematics to analyse the systems. Third, we consider the first ever discovered lens system Q0957+561 at  $z = 0.36$ , which is the best studied lens system including a cluster for the lens potential. The velocity dispersion for the central galaxy is reported by Tonry & Franx (1999). The virial mass of the cluster is from Nakajima et al. (2009) who derive the halo mass through weak lensing and find that their result is consistent with the result by Chartas et al. (2002) through X-ray observations. Finally, we consider galaxy cluster Abell 611 that has been studied extensively by Newman et al. (2009) through a combination of strong and weak lensing and stellar kinematics. As shown in Fig. 3 these individual measurements are in excellent agreement with the  $M_{\text{vir}}-\sigma$  relation based on the abundance matching of statistical functions. This agreement bolsters the validity of the  $M_{\text{vir}}-\sigma$  relation at  $z = 0$ .

Notice that the  $M_{\text{vir}}-\sigma$  relation shown in Fig. 3 is a curve rather than a straight line. Consequently, it does not match well the prediction by the singular isothermal sphere

<sup>2</sup> This correction has only a relatively minor effect, in particular for large mass.

<sup>3</sup> The Andromeda galaxy is also a well-studied example, but the inferred virial masses appear to still vary by a factor of 2 (e.g., Klypin et al. 2002; Seigar et al. 2008).

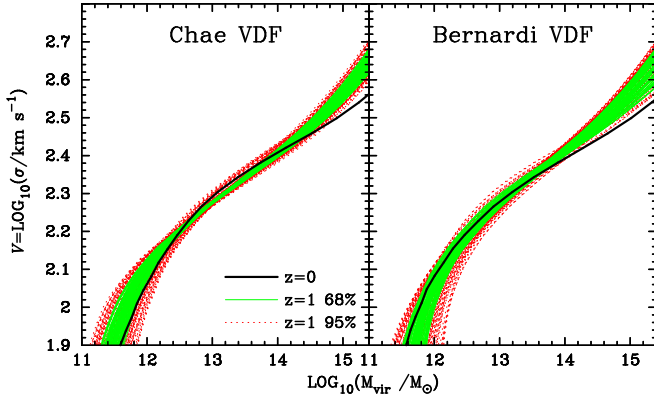


**Figure 4.** The abundance matching  $M_{\text{vir}}-\sigma$  relation at  $z = 1$  is compared with that at  $z = 0$ . It is consistent with zero evolution between  $z = 1$  and  $z = 0$  for the strong lensing probed range  $\sigma \lesssim 300 \text{ km s}^{-1}$  ( $M_{\text{vir}} \lesssim 10^{14.6} M_{\odot}$ ; see §2).

(SIS) halo model (see, e.g., Li & Ostriker 2002). The failure of the SIS model is evident for  $M_{\text{vir}} \gtrsim 10^{13} M_{\odot}$  as noticed by several authors (e.g. Li & Ostriker 2002; Kochanek & White 2001; Blumenthal et al. 1986). This result confirms the critical halo mass  $M_c \sim 10^{13} M_{\odot}$  below which the baryonic effects start to become significant for the inner halo dynamics and structure. However, even for  $M_{\text{vir}} \lesssim 10^{13} M_{\odot}$  the SIS model is not very successful in matching the empirically determined  $\sigma(M_{\text{vir}})$  curve. This implies that the SIS model is not precise as a ‘global model’ of the galactic halo despite the fact that a range of observational constraints support the isothermal profile for the inner part of the halo (see Chae 2010 and references therein). The underprediction of  $\sigma$  by the SIS model for  $M_{\text{vir}} \lesssim 10^{13} M_{\odot}$  probably reflects the neglected concentration of the halo. The curvature in the  $M_{\text{vir}}-\sigma$  relation may reflect the systematic variation of halo concentration but may also imply the varying baryonic effects on the halo structures. The internal structures of the haloes may be constrained by combining dynamical constraints with the empirical  $M_{\text{vir}}-\sigma$  relation (in preparation).

### 3.2 The coevolution of the HMF and the VDF

In Fig. 4 we compare the abundance matching  $M_{\text{vir}}-\sigma$  relations at  $z = 1$  and 0. This comparison shows little sign of evolution in the  $M_{\text{vir}}-\sigma$  relation for the strong lensing probed range  $\sigma \lesssim 300 \text{ km s}^{-1}$  ( $M_{\text{vir}} \lesssim 10^{14.6} M_{\odot}$ ; see §2). The near constancy in the  $M_{\text{vir}}-\sigma$  relation with  $z$  implies that the HMF and the VDF are coevolving in parallel. Namely, as the halo grows in mass over cosmic time, the central stellar velocity dispersion grows in accordance. The natural question to ask is then what the origin of this coevolution is. We discuss this in §5.

Alternatively, we may transform the HMF into a VDF using the  $z = 0$  relation of Fig. 4 and assuming a certain evolution of the  $M_{\text{vir}}-\sigma$  relation. Fig. 5 shows the VDFs predicted from the HMFs assuming zero evolution of the  $M_{\text{vir}}-\sigma$  relation. In Fig. 5 the HMF-converted VDFs are compared

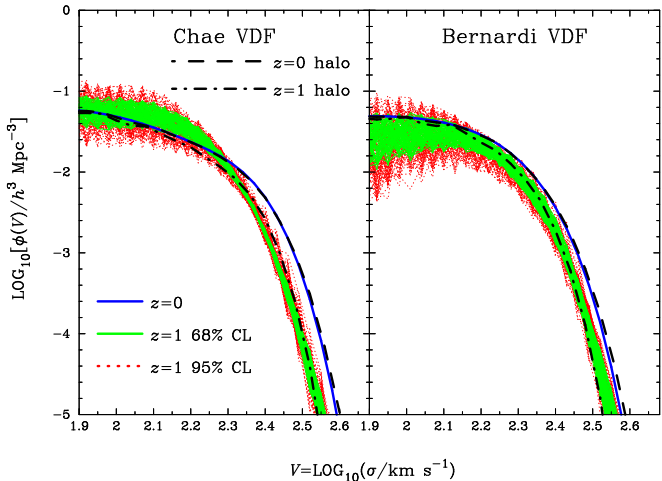


**Figure 5.** The observationally constrained VDFs at  $z = 0$  and  $z = 1$  are compared with the VDFs predicted from the  $\Lambda$ CDM halo mass function using the empirically determined relation  $\sigma(M_{\text{vir}})$  at  $z = 0$  assuming zero evolution (see Fig. 4). There is a reasonably good match between the observationally derived VDF evolution and the halo-predicted VDF evolution.

with the observationally derived local VDFs and the lensing constrained VDFs at  $z = 1$ . The VDFs at  $z = 0$  are in excellent agreement with each other. The VDFs at  $z = 1$  are also in agreement with each other. This exercise shows that under the simple assumption of the constancy of the  $M_{\text{vir}}-\sigma$  relation in time, the evolution of the HMF predicted by the current  $\Lambda$ CDM cosmology can match well the evolution of the VDF constrained by strong lensing statistics for  $0 \lesssim z \lesssim 1$ .

### 4 CONNECTION BETWEEN THE OBSERVATIONAL VDF AND THE SMF FROM GALAXY SURVEYS

Many recent surveys of galaxies have been used to constrain the evolution of galaxies through the LF or/and the SMF. The results are at variance. Many results argue for relatively little evolution in the number density of most massive galaxies and greater evolution of less massive galaxies over cosmic time, i.e. a “stellar mass-downsizing” (anti-hierarchical) behaviour (e.g., Cimatti et al. 2006; Fontana et al. 2006; Pozzetti et al. 2007; Conselice et al. 2007; Scarlata et al. 2007; Cool et al. 2008; Pérez-González et al. 2008; Marchesini et al. 2009), although there are results that do not particularly support a mass-downsizing evolution (e.g., Bell et al. 2004; Faber et al. 2007; Brown et al. 2008; Ilbert et al. 2010). The variance for the evolution of the SMF is not well understood but may be due to errors in measurements and modelling of the SMF (see Longhetti & Saracco 2009) and galaxy sample biases caused by cosmic variance (see, e.g., Faber et al. 2007; Cattaneo et al. 2008; Stringer et al. 2009 for discussions).

We have seen in the previous section that the strong lensing constrained VDF evolution is in line with the theoretical HMF evolution. How well would the VDF match the

observed SMF from galaxy surveys? What would be the correlation between stellar mass ( $M_*$ ) and velocity dispersion ( $\sigma$ ) and its evolution up to  $z = 1$ ? The coevolution of the SMF and the VDF will depend on the evolution of the  $M_*$ - $\sigma$  relation. Hence the evolution of the VDF can be tested against the evolution of the SMF only when the  $M_*$ - $\sigma$  relation is known (or assumed) as a function of cosmic time. Conversely, by matching the observed SMF evolution from galaxy surveys with the VDF evolution from strong lensing statistics we may infer the evolution of the  $M_*$ - $\sigma$  relation. In the following we take the latter approach.

We match the VDFs by Chae (2010) and Bernardi et al. (2010) (their evolutions being constrained by strong lensing) with two total SMFs from galaxy surveys (see Fig. 2) that are qualitatively different and are intended to encompass the current range of observations. One is the COSMOS SMF by Ilbert et al. (2010) measured using 192,000 galaxies from the COSMOS 2-deg<sup>2</sup> field. The COSMOS sample size is much larger than any other single data set that has been used to derive the SMF up to  $z \gtrsim 1$ . For the Ilbert et al. (2010) SMF  $z = 0$  function is actually for  $0.2 < z < 0.4$  while  $z = 1$  function is a mean of  $0.8 < z < 1.0$  and  $1.0 < z < 1.2$  functions. Notice that the Ilbert et al. (2010) SMF does not show a stellar mass-downsizing evolution. The other is the Spitzer SMF by Pérez-González et al. (2008).<sup>4</sup> This is a typical SMF that shows a downsizing behaviour. For the Pérez-González et al. (2008) SMF  $z = 0$  function is actually for  $0 < z < 0.2$  while  $z = 1$  function is a mean of  $0.8 < z < 1.0$  and  $1.0 < z < 1.3$  functions. We note that the Pérez-González et al. (2008) sample covers a sky area of only  $\sim 664$  arcmin<sup>2</sup> and contains  $\sim 28,000$  sources for  $0 < z < 4$ .

#### 4.1 The $M_*$ - $\sigma$ relation at $z = 0$

Fig. 6 shows several examples of the abundance matching relation between  $M_*$  and  $\sigma$  at  $z = 0$ . For  $z = 0$  only we consider the Bernardi et al. (2010) SMF as well as the COSMOS and the Spitzer SMFs. These results have been obtained taking into account the effect of an adopted intrinsic scatter (the region shaded green) for  $V \equiv \log_{10}(\sigma / \text{km s}^{-1})$  of  $0.115 - 0.039 \times (m - 10)$  with  $m \equiv \log_{10}(M_*/M_\odot)$  from Desroches et al. (2007) (see Appendix A). The details on the effect of the intrinsic scatter can be found in Appendix A. Notice that the abundance matching  $M_*$ - $\sigma$  relations have mild curvatures. For a linear approximation  $V = bm + \text{const}$ , the slope  $b$  varies from  $b = [0.23, 0.34]$  for  $m > 11.5$  to  $b = [0.35, 0.49]$  for  $m < 10.5$ . The abundance matching relations for all galaxies are compared with the directly measured median relations for early-type galaxies in the literature (Desroches et al. 2007; Hyde & Bernardi 2009; Shankar et al. 2010). The abundance matching relations agree well with the early-type relations for  $M_* \gtrsim 10^{11.6} M_\odot$ . However, as  $M_*$  decreases, the abundance matching relations deviate systematically and increasingly from the early-type relations. This is expected and can be well understood by the fact that the late-type relation is different from the

<sup>4</sup> Pérez-González et al. (2008) adopt the Salpeter IMF to calculate their stellar masses. To convert their stellar masses to those based on the Chabrier IMF, we divide by 1.7.

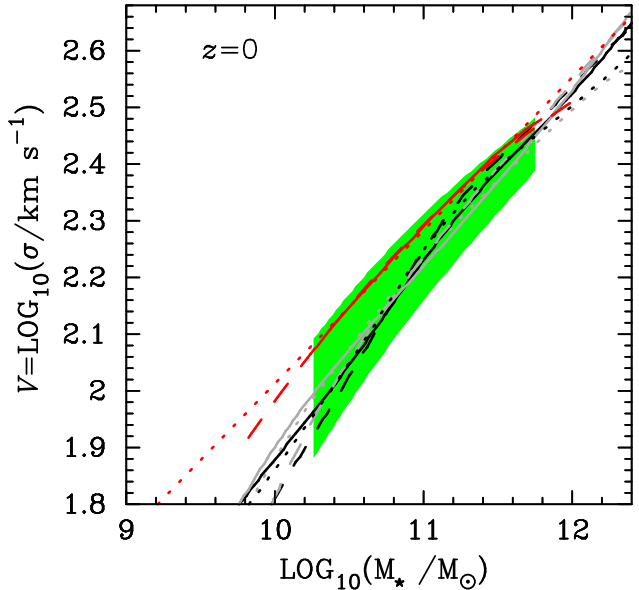


**Figure 6.** The abundance matching relation between the stellar mass ( $M_*$ ) and the stellar velocity dispersion ( $\sigma$ ) of galaxies at  $z = 0$ . Black (gray) solid, dashed, and dotted curves are respectively the results of matching the Chae (2010) (Bernardi et al. 2010) VDF with the COSMOS SMF by Ilbert et al. (2010), the Spitzer SMF by Pérez-González et al. (2008), and the SDSS SMF by Bernardi et al. (2010) for all galaxies. These abundance matching results have been corrected for the effects of the intrinsic scatter shaded green. The intrinsic scatter and its effects are described in Appendix A. The red solid, dashed and dotted curves/lines are the measured median  $M_*$ - $\sigma$  relations respectively by Desroches et al. (2007), Hyde & Bernardi (2009), and Shankar et al. (2010) for early-type galaxies. Notice that the abundance matching relations agree well with the measured early-type relations at high  $M_*$  but deviate systematically as  $M_*$  gets lower because the late-type contribution becomes increasingly larger.

early-type relation and the late-type contribution to the total relation increases as  $M_*$  decreases.

#### 4.2 The $M_*$ - $\sigma$ relation at $z = 1$ and its evolution to $z = 0$

In Fig. 7, the abundance matching  $M_*$ - $\sigma$  relation at  $z = 1$  is shown and compared with that at  $z = 0$ . The relation at  $z = 1$  is also compared against the individual data points for  $0.7 < z < 1.3$  from di Serego Alighieri (2005) and van der Wel et al. (2005). The resulting evolution of the  $M_*$ - $\sigma$  relation varies depending mostly on the adopted SMF. Notice that the strictly valid range probed by the data is  $1.97 \lesssim V[\equiv \log_{10}(\sigma / \text{km s}^{-1})] \lesssim 2.47$  corresponding to  $10.2 \lesssim m[\equiv \log_{10}(M_*/M_\odot)] \lesssim 11.8$  (see §2). The results outside this range are extrapolations.

For the COSMOS SMF the  $M_*$ - $\sigma$  relation is consistent with zero evolution. The relation at  $z = 1$  is also consistent with the measured data points. On the other hand, for the Spitzer SMF (a typical downsizing SMF) the  $z = 1$  relation deviates systematically from the  $z = 0$  relation in particular for massive galaxies with  $M_* \gtrsim 10^{11} M_\odot$ . This appears to be the case for any downsizing SMF. This is because the evolu-

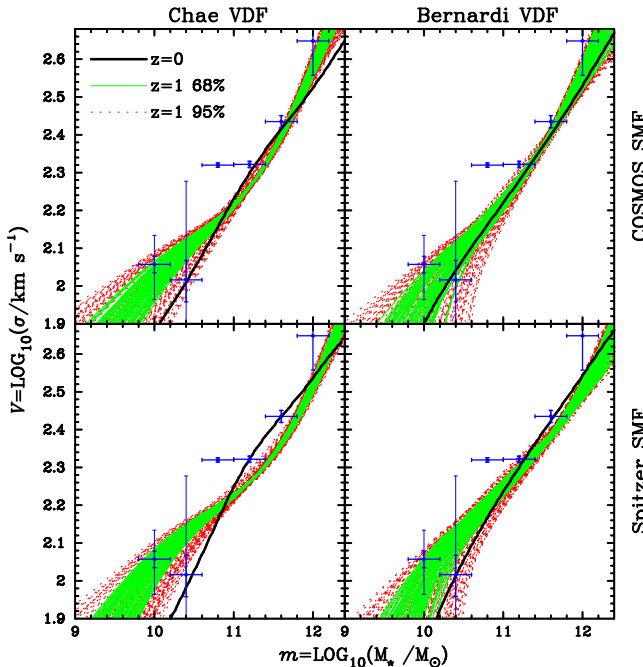


**Figure 7.** The  $M_*$ - $\sigma$  relation at  $z = 1$  is compared with that at  $z = 0$ , inferred from the abundance matching of the strong lensing constrained evolutions of the VDFs of Chae (2010) and Bernardi et al. (2010) with the observed SMFs from galaxy surveys (see the texts in §4). Two SMFs are used: the COSMOS SMF by Ilbert et al. (2010) and the Spitzer SMF by Pérez-González et al. (2008). The blue data points are the weighted means and their errors (thin error bars are dispersions) for mass intervals of 0.4 dex based on 47 galaxies for  $0.7 < z < 1.3$  from di Serego Alighieri (2005) and van der Wel et al. (2005). All stellar masses are for the Chabrier IMF.

tionary behaviour of a downsizing SMF is dissimilar to that of the VDF. This implies that a downsizing SMF requires a differential evolution in the  $M_*$ - $\sigma$  relation. In particular, according to the downsizing SMF  $\sigma$  has to be lower at  $z = 1$  than  $z = 0$  at fixed  $M_*$  ( $\gtrsim 10^{11.2-11.4} M_\odot$ ).

Then, which of the above cases (the non-evolving or the evolving case) of the  $M_*$ - $\sigma$  relation would be more consistent with other independent results on the structural evolutions of galaxies?

#### 4.2.1 Comparison with observed structural evolutions of galaxies

According to recent studies on the structural evolutions of galaxies, there are observational indications that galaxy size evolves at fixed stellar mass (e.g. Trujillo et al. 2007; van der Wel et al. 2008; Cimatti et al. 2008; van Dokkum et al. 2008; Bezanson et al. 2009). However, more recent studies find that physical mass densities (as opposed to effective densities) evolve little (Hopkins et al. 2009a; Bezanson et al. 2009). This implies that velocity dispersion might evolve little at fixed stellar mass. Indeed, Cenarro & Trujillo (2009) find a slow evolution of  $\sigma(M_*)$  since  $z \sim 1.6$  from an analysis of spectra of massive galaxies (see also Cappellari et al. 2009). Nev-

ertheless, Cenarro & Trujillo (2009) find a higher  $\sigma$  at a higher  $z$  for  $0.5 \times 10^{11} M_\odot \lesssim M_* \lesssim 2 \times 10^{11} M_\odot$  (an evolution from  $\sigma \sim 180 \text{ km s}^{-1}$  at  $z \sim 0$  to  $\sim 240 \text{ km s}^{-1}$  at 1.6). However, as shown in Fig. 8 a similar data set actually appears to indicate no evolution at all. The velocity dispersion at a fixed stellar mass of  $M_* = 10^{11} M_\odot$  rather than a range stays constant at  $\sigma \approx 210 \text{ km s}^{-1}$  between  $z \sim 0$  and  $\sim 1.8$ . Notice that we only use galaxies with  $10.75 < \log_{10}(M_*/M_\odot) < 11.25$  and we convert the measured value of  $\sigma$  at the measured value of  $M_*$  for each galaxy to that at  $M_* = 10^{11} M_\odot$  using an empirical relation found in Fig. 6. This prescription largely removes any systematic error arising from the differences in the stellar masses of the galaxies in the different redshift bins. Another difference between the Cenarro & Trujillo (2009) analysis and ours is that for local galaxies Cenarro & Trujillo (2009) use SDSS DR6 data to derive stellar masses while we use only SLACS galaxies for which two independent stellar mass measurements are available based on SDSS (Grillo et al. 2009) and HST (Auger et al. 2009) photometric data.

Incidentally, all the abundance matching results shown in Fig. 7 imply no or little evolution of  $\sigma(z)$  at  $M_* = 10^{11} M_\odot$  regardless of the VDF or the SMF used. Hence, our abundance matching results are in excellent agreement with, but at the same time are not distinguished by, our analysis of the data from the literature for individual galaxies for  $0 \lesssim z \lesssim 2$ . However, it is important to notice that none of the current observational results on the structural evolutions of galaxies indicate a negative evolution in  $\sigma$  with  $z$  for any  $M_*$ . Observational indications (e.g. stellar mass densities) are such that velocity dispersions cannot be lower at a higher  $z$  in case of evolution. Hence, according to our abundance matching results the downsizing SMF is inconsistent with the VDF evolution from strong lensing by Chae (2010) because it requires a lower  $\sigma$  at a higher  $z$  for massive galaxies.

#### 4.2.2 Comparison with predictions from cosmological hydrodynamic simulations

At fixed stellar mass cosmological hydrodynamic simulations from the literature also find slow or little evolutions of velocity dispersion. For example, Hopkins et al. (2009b) combine dark halo merging with hydrodynamic simulation results and observed empirical properties of galaxies to find little evolutions of  $\sigma(z)$  at fixed  $M_*$  (Fig. 8). Hopkins et al. (2010) find slow evolutions through more realistic cosmological simulations taking into account various effects including equal and minor merging, adiabatic expansion and observational effects (Fig. 8). Cenarro & Trujillo (2009) predict based on the Hopkins et al. (2009b) model a somewhat greater evolution using their analysis of spheroid size evolutions (Fig. 8). These simulations are broadly consistent with the constraints from the current data as analysed above (Fig. 8) and the abundance matching results (Fig. 7) in the sense that the predicted evolutions are slow and can be made in principle to agree with the observational constraints. Furthermore, Hopkins et al. (2009b) find that the evolution of  $\sigma(z)$  at fixed  $M_*$  has little sensitivity on  $M_*$  for  $10^9 M_\odot \lesssim M_* \lesssim 10^{12} M_\odot$ . These simulation results are consistent with our abundance matching results based on the non-downsizing SMF but not with the downsizing SMF.

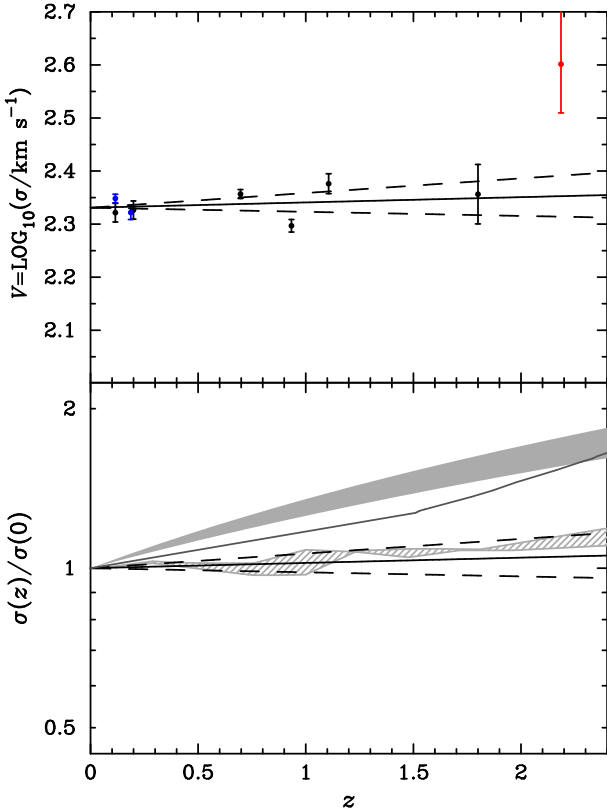


**Figure 8.** *Upper panel:* The observed stellar velocity dispersion ( $\sigma$ ) as a function of  $z$  at fixed stellar mass  $M_\star = 10^{11} M_\odot$ . The data points are based on galaxies with measured stellar masses in the range  $10.75 < m[\equiv \log_{10}(M_\star/M_\odot)] < 11.25$ . Furthermore, to estimate the velocity dispersion at  $m = 11$  as precisely as possible we use an empirical relation of  $V = bm + \text{const}$  where  $V = \log_{10}(\sigma/\text{km s}^{-1})$  and we take  $b = 0.34$  as estimated from Fig. 6 for  $10.75 < m < 11.25$  (the results are insensitive to the exact value of  $b$  for  $b > 0.2$ ). The references for the data are as follows: (1)  $z < 0.15$ , 8 (or 17 for blue point) galaxies – Bolton et al. (2008) & Grillo et al. (2009) (or Auger et al. (2009)) (2)  $0.15 \leq z < 0.4$ , 9 (or 11 for blue point) galaxies – Bolton et al. (2008) & Grillo et al. (2009) (or Auger et al. (2009)) (3)  $0.6 \leq z < 0.8$ , 7 galaxies – van der Wel et al. (2005) (4)  $0.8 \leq z < 1.0$ , 10 galaxies – van der Wel et al. (2005), di Serego Alighieri (2005) (5)  $1.0 \leq z < 1.3$ , 8 galaxies – van der Wel et al. (2005), di Serego Alighieri (2005) (6)  $1.6 \leq z < 1.8$ , 7 galaxies – Cappellari et al. (2009), (7)  $z=2.186$ , 1 galaxy (red point) – van Dokkum et al. (2009). The solid line is the best-fit in the least-square fit of the data points and the dashed lines represent the errors in the slope. The single galaxy at  $z=2.186$  is not used for the fit but consistent with the fit result at the  $2\sigma$  level. *Lower panel:* The evolution factor of the velocity dispersion as a function of  $z$ . The black solid and dashed lines are the fit results from the upper panel. The light hatched area is the prediction by Hopkins et al. (2009b). The light gray area is the result based on the Hopkins et al. (2009b) model presented by Cenarro & Trujillo (2009) who use local SDSS data and similar data for  $z > 0.5$  as used here but without converting the measured velocity dispersions to the values at a fixed stellar mass (they use a broad range  $0.5 \times 10^{11} M_\odot \lesssim M_\star \lesssim 2 \times 10^{11} M_\odot$ ). The dark gray solid curve is the prediction by Hopkins et al. (2010).

To sum up, our abundance matching results based on the non-downsizing SMF are broadly consistent with observational constraints on the structural evolutions of galaxies and cosmological hydrodynamic simulation results. However, the downsizing SMF gives a differential evolution in  $\sigma(M_\star)$  with  $z$  that would not be consistent with observational constraints or simulation results.

## 5 IMPLICATIONS FOR THE $\Lambda$ CDM PARADIGM AND GALAXY EVOLUTION

At the heart of the current hierarchical structure formation theory is the bottom-up build-up of dark matter haloes. Given that galaxies are believed to be born and centered in those haloes, what would be the evolutionary patterns of galaxies? Unlike dark haloes, galaxies have two distinctive properties, namely, the photometric property and the dynamical property. Hence, there are two evolutionary properties of galaxies to be considered. The star formation history of galaxies gives rise to above all the evolutionary patterns in the luminosity and stellar mass functions of galaxies. Most cosmological observations have been devoted to the photometric properties. Galaxy formation models, whether semi-analytical or hydrodynamical, have also tried to reproduce the photometric properties rich in observational data. Notice that dark haloes do not have such photometric properties. This means that connections between the photometric properties of galaxies and dark haloes are indirect and challenging. Galaxy evolution in its dynamical property, which is the focus of this work, may be characterized by the evolutionary patterns in the velocity (dispersion) functions of galaxies. One may wonder whether the dynamical property of galaxies may be more intimately linked to dark haloes than the photometric properties do. How is the dynamical property of galaxy evolution related to dark haloes? What would be the role of the photometric property of galaxy evolution in this context?

Current galaxy formation models cannot yet reliably predict central dynamical properties of galaxies. In this work we have compared the lensing-constrained evolution of the VDF with the  $\Lambda$ CDM predicted evolution of the HMF and the observed evolution of the SMF. The main result is that the halo virial mass ( $M_{\text{vir}}$ ), the galaxy stellar mass ( $M_\star$ ) and the central line-of-sight stellar velocity dispersion ( $\sigma$ ) are positively coevolving for the probed redshift range of  $0 \lesssim z \lesssim 1$ . What are the implications of the results from this work for galaxy formation and evolution under the  $\Lambda$ CDM hierarchical paradigm?

**Halo mass-velocity dispersion relation:** We find that  $M_{\text{vir}}-\sigma$  relation does not evolve between  $z = 1$  and  $z = 0$  (Fig. 4) for the entire probed range of halo mass from galactic haloes to cluster haloes. This empirical finding is insensitive to the choice of the HMF and the VDF from current simulations and observations under a concordance  $\Lambda$ CDM cosmological model.

Pure dark halo simulations predict that a halo of mass  $M_{\text{vir}}$  at  $z = 1$  is smaller (i.e. smaller  $R_{\text{vir}}$ ) but less concentrated (i.e. smaller  $c_{\text{vir}}$ ) than that at  $z = 0$ . As to the central velocity dispersion the two effects are opposite so that we may expect  $\sigma(M_{\text{vir}})$  to evolve little as far as pure haloes are concerned. Let us consider this quantitatively using a

simple model. Without dissipational galaxy formation, the evolution of the central velocity dispersion would be primarily determined by the evolutions of the virial mass ( $M_{\text{vir}}$ ), the virial radius ( $r_{\text{vir}}$ ) and the concentration ( $c_{\text{vir}}$ ). The velocity dispersion is expected to increase (decrease, increase) if  $M_{\text{vir}}$  ( $r_{\text{vir}}, c_{\text{vir}}$ ) increases while the other two parameters are held constant. Cosmological  $N$ -body simulations predict that all three parameters (i.e.  $M_{\text{vir}}$ ,  $r_{\text{vir}}$  and  $c_{\text{vir}}$ ) increase as cosmic time evolves forward. Suppose  $\sigma = v_{\text{vir}} f(c_{\text{vir}}, r/r_{\text{vir}})$  where  $\sigma$  is the velocity dispersion in the central region (e.g. within  $0.01r_{\text{vir}}$ ),  $v_{\text{vir}} = \sqrt{GM_{\text{vir}}/r_{\text{vir}}}$  is the circular velocity at the virial radius, and  $f(c_{\text{vir}}, r/r_{\text{vir}})$  is a model-dependent factor relating the two.  $N$ -body simulations show that  $M_{\text{vir}}$ ,  $r_{\text{vir}}$  and  $c_{\text{vir}}$  all increase roughly by a factor of 2 from  $z = 1$  to 0 (see, e.g., Wechsler et al. 2002). Then,  $v_{\text{vir}}$  stays roughly constant and  $f(c_{\text{vir}}, r/r_{\text{vir}})$  increases by about 15% from  $z = 1$  to 0 for an isotropic NFW model (see Lokas & Mamon 2001). Hence we expect some enhancement in the velocity dispersion (i.e. a positive coevolution) in the course of the hierarchical growth of a pure dark halo from  $z = 1$  to 0.

For realistic haloes hosting (dissipationally formed) galaxies hydrodynamic simulations can be used to predict the evolution of  $\sigma(M_{\text{vir}})$ . Unfortunately, current hydrodynamic simulations do not predict robustly the baryonic effects on halo structures (e.g. Blumenthal et al. 1986; Gnedin et al. 2004; Abadi et al. 2009; Tissera et al. 2010; Feldmann et al. 2010). Specifically, recent hydrodynamic simulations overpredict  $\sigma$  at a given  $M_{\text{vir}}$  (e.g. Tissera et al. 2010; Feldmann et al. 2010).

The finding that the  $M_{\text{vir}}-\sigma$  relation does not evolve for  $0 \leq z \leq 1$  offers new insights into galaxy formation and evolution. It implies that the dynamical property of the central galaxy of a halo has little to do with its history but is dictated by the final halo virial mass at least since  $z = 1$ . Remarkably, this is the case for all haloes probed (with  $\sigma \gtrsim 100 \text{ km s}^{-1}$ ). Implications of this finding are discussed below in the context of the coevolution of  $M_{\text{vir}}$ ,  $\sigma$  and  $M_{\star}$ .

**Stellar mass-velocity dispersion relation:** The  $M_{\star}-\sigma$  relation at  $z = 0$  shows a power-law relation  $M_{\star} \propto \sigma^{\gamma_{\text{SM}}}$  with a varying power-law index  $\gamma_{\text{SM}}$  ranging from [2.9, 4.4] for  $M_{\star} > 10^{11.5} M_{\odot}$  to [2.0, 2.9] for  $M_{\star} < 10^{10.5} M_{\odot}$ . Let us compare the  $M_{\star}-\sigma$  relation with power-law correlations between luminosity and internal velocity parameter, namely the Tully-Fisher relation for the late-type population and the Faber-Jackson relation for the early-type population. The observed Tully-Fisher relation exponent  $\gamma_{\text{TF}}$  lies between 2.5 and 3.5 (see §2.3 or Pizagno et al. 2007). The traditional value for the Faber-Jackson exponent  $\gamma_{\text{FJ}}$  for early-type galaxies is  $\approx 4$ . However, an extensive analysis of SDSS DR5 early-type galaxies reveals that  $\gamma_{\text{FJ}}$  varies systematically from  $2.7 \pm 0.2$  at  $L_{\star}$  to  $4.6 \pm 0.4$  at the upper luminosity end (Choi et al. 2007; see also Desroches et al. 2007). The abundance matching  $M_{\star}-\sigma$  relation for all galaxies can match well these Faber-Jackson/Tully-Fisher relations in conjunction with measured  $M_{\star}/L$  ratios (e.g. Bell et al. 2003).

In Fig. 7 the  $M_{\star}-\sigma$  relation at  $z = 1$  is compared with that at  $z = 0$  based on two VDFs and two SMFs that are meant to encompass the current range of observations. As can be seen in the figure, the implied evolution depends sensitively on the adopted SMF and to a less degree on the adopted VDF. The relation based on the COSMOS SMF is

consistent with zero evolution in  $\sigma(M_{\star})$  between  $z = 1$  and 0. On the other hand, the relation based on the Spitzer SMF (a typical downsizing SMF) implies a differential evolution in  $\sigma(M_{\star})$ : for  $M_{\star} \gtrsim 10^{11} M_{\odot}$  the implied evolution in  $\sigma$  with redshift at fixed  $M_{\star}$  is negative while it is positive for  $M_{\star} \lesssim 10^{11} M_{\odot}$ . This means that based on the downsizing SMF a galaxy at  $z = 1$  would have a shallower (steeper) mass profile than the local counterpart of the same stellar mass for  $M_{\star} \gtrsim 10^{11} M_{\odot}$  ( $M_{\star} \lesssim 10^{11} M_{\odot}$ ).

How the above results on the evolution in  $\sigma(M_{\star})$  are compared with other independent results on the structural evolutions of galaxies? First of all, we find little evolution in  $\sigma(z)$  at  $M_{\star} = 10^{11} M_{\odot}$  for  $0 \lesssim z \lesssim 1.8$  from a careful analysis of the data in the literature (see Fig. 8). This is in excellent agreement with the above abundance matching results. However, it cannot unfortunately distinguish the abundance matching results because  $M_{\star} = 10^{11} M_{\odot}$  happens to be the critical mass for the downsizing SMF at which the evolution changes the sign. Second, many observational studies find a negative size evolution of galaxies with redshift implying a more steeply declining stellar mass profile at a higher  $z$  (e.g. Trujillo et al. 2007; van der Wel et al. 2008; Cimatti et al. 2008; van Dokkum et al. 2008). However, more recent studies find that stellar mass density profiles of the inner regions up to several kilo-parsecs are consistent with no evolution for massive galaxies with  $M_{\star} \gtrsim 10^{11} M_{\odot}$  (Hopkins et al. 2009a; Bezanson et al. 2009). According to these studies, however, it is not clear whether stellar mass density profiles evolve beyond the inner regions. Whatever the case these results can only imply a similar or larger  $\sigma$  at fixed  $M_{\star}$  at a higher redshift contradicting the abundance matching results based on the downsizing SMF.

What do hydrodynamic simulations predict on the evolution of the relation between  $M_{\star}$  and  $\sigma$ ? Hopkins et al. (2009b) combine galaxy merging with hydrodynamic simulation to find a little evolution of  $\sigma$  with  $z$  at fixed  $M_{\star}$  for any  $10^9 M_{\odot} \leq M_{\star} \leq 10^{12} M_{\odot}$ . In particular, Hopkins et al. (2009b) explicitly predict that the  $M_{\star}-\sigma$  relation evolves little between  $z = 1$  and 0. Hopkins et al. (2010) take into account a number of possible effects in their cosmological simulations and find slow evolutions of  $\sigma$  with  $z$ . These results are consistent with the evolution in  $\sigma(M_{\star})$  with  $z$  based on the COSMOS SMF but not with the downsizing SMF.

**VDF evolution: concord or conflict with observed galaxy evolutions?** We have already compared the evolving VDF with the evolving HMF and the evolving SMF. We find that the evolutions of the HMF, the VDF and the SMF appear concordant, but that the downsizing SMF is disfavoured because its implied structural evolutions are unlikely. It is clearly worthwhile to put the VDF evolution in a broader context of recent cosmological observations on galaxy evolutions.

The lensing constrained VDF evolutions show that the number density of massive early-type galaxies ( $\sigma \gtrsim 220 \text{ km s}^{-1}$ ) not only evolves significantly but also shows a differential evolution (see Fig. 1): the higher the velocity dispersion, the faster the number density evolution (the ‘‘velocity-upsizing’’ behaviour), probably meaning an ‘‘mass-upsizing’’ behaviour (i.e. the behaviour of more massive galaxies assembling later in cosmic time). Matsuoka & Kawara (2010) has just recently compiled a large number ( $\sim 60,000$ ) of massive galaxies ( $M_{\star} >$

$10^{11} M_{\odot}$ ) over a large sky area ( $55.2 \text{ deg}^2$ ) from the UKIRT Infrared Deep Sky Survey (UKIDSS) and the SDSS II Supernova Survey. Matsuoka & Kawara (2010) find a significantly greater number density evolution for  $M_{\star} > 10^{11.5} M_{\odot}$  than  $M_{\star} < 10^{11.5} M_{\odot}$  out to  $z = 1$  consistent with the hierarchical evolution. The parallel evolution of the VDF and the SMF would imply no evolution in the total mass profile of galaxies. Indeed, strong lens modelling (Koopmans et al. 2006; Saha et al. 2007; Winn et al. 2004; Treu & Koopmans 2002) and velocity dispersion measurements to a high redshift (Fig. 8) support non-evolution in total mass profiles even if stellar mass profiles evolve. Galaxy merging is an independent route to probe the build-up of galaxies over cosmic time (e.g. White et al. 2007; Masjedi et al. 2008; Wake et al. 2008; de Ravel et al. 2009; Bundy et al. 2009). The mere fact that thousands of merging events have been observed is the evidence for some sort of hierarchical mass assembly going on. The issue is the merging rate and its dependence on galaxy mass. Observed merging rates are at variance and cannot test the hierarchical assembly of massive galaxies robustly. It is, however, worth noting the more recent result by Bundy et al. (2009) that merging rate is greater for massive galaxies with  $M_{\star} > 10^{11} M_{\odot}$  than less massive galaxies. The Bundy et al. (2009) result is in line with the hierarchical mass assembly and agrees qualitatively with the VDF evolution.

*Coevolution of  $M_{\text{vir}}$ ,  $\sigma$  and  $M_{\star}$  and implications for the  $\Lambda$ CDM paradigm:* In the above discussions we have considered the connections of  $\sigma$  with  $M_{\text{vir}}$  and  $M_{\star}$  separately. The results that  $\sigma$  is coevolving in parallel with both  $M_{\text{vir}}$  and  $M_{\star}$  necessarily imply a similar coevolution of  $M_{\text{vir}}$  and  $M_{\star}$ . Fig. 9 shows the abundance matching  $M_{\text{vir}}-M_{\star}$  relations at  $z = 0$  and  $z = 1$ . The results based on the COSMOS SMF give little evolution in the  $M_{\text{vir}}-M_{\star}$  relation for  $M_{\text{vir}} \gtrsim 10^{12} M_{\odot}$  implying a parallel coevolution of  $M_{\text{vir}}$  and  $M_{\star}$  with cosmic time. This is consistent with the little evolutions in the  $M_{\text{vir}}-\sigma$  and the  $M_{\star}-\sigma$  relations based on the same SMF. Hence, we are left with the simple picture that  $M_{\text{vir}}$ ,  $M_{\star}$  and  $\sigma$  are all coevolving so that a halo of given mass  $\gtrsim 10^{12} M_{\odot}$  has on average the same stellar mass and the same stellar velocity dispersion for its central galaxy independent of redshift for  $0 \lesssim z \lesssim 1$ . Some indications of evolution in the  $M_{\text{vir}}-M_{\star}$  relation (and possibly in the  $M_{\star}-\sigma$  relation) for  $M_{\text{vir}} \lesssim 10^{12} M_{\odot}$  may imply a differential evolution among  $M_{\text{vir}}$ ,  $M_{\star}$  and  $\sigma$ . We cannot address this issue for low-mass haloes here because the strong lensing constrained VDF evolution from this work breaks down at low  $\sigma$ . The results based on the (downsizing) Spitzer SMF give a mild differential evolution in the  $M_{\text{vir}}-M_{\star}$  relation at large masses<sup>5</sup> as it is the case for  $M_{\star}-\sigma$  relation. However, in the above we have argued that a downsizing SMF is unlikely.

How the parent dark halo is dynamically related to the residing galaxy as a function of cosmic time is a fundamental question for galaxy formation and evolution. In this work we have studied the connection of the halo mass ( $M_{\text{vir}}$ ) with the stellar velocity dispersion ( $\sigma$ ) and the stellar mass ( $M_{\star}$ ) of the central galaxy for  $0 \lesssim z \lesssim 1$ . According to our results

the stellar dynamics in the galaxy (characterized by  $\sigma$ ) is closely linked to the parent halo mass  $M_{\text{vir}}$  independent of redshift for  $0 \lesssim z \lesssim 1$ . A link between the central particle velocity dispersion and  $M_{\text{vir}}$  is expected in the  $\Lambda$ CDM paradigm because it predicts on average a universal density profile independent of  $M_{\text{vir}}$  (e.g. Navarro et al. 2004, 2010 and references therein) along with well-defined scaling relations of the structural parameters with  $M_{\text{vir}}$  (e.g. Bullock et al. 2001; Macciò et al. 2007; Klypin et al. 2010). According to the coevolution, dissipational baryonic physics involving star formation that may have modified the central potential of the halo has not destroyed but appears to have refined the link.

It is then natural to suggest that dissipational baryonic physics results in on average a rescaled universal (or universal class) density profile of the stellar plus dark mass distribution, or perhaps more realistically a universal (class) density profile of dark matter combined with a well-correlated class of stellar mass distribution. What would then the baryon-modified universal (class) density profile look like? The observation that the inner density profile of the galaxy plus halo system is on average close to isothermal (see Chae 2010 for a review and references) combined with the expectation that baryonic effects are not likely to be important well outside the scale radii (e.g. Gnedin et al. 2004; Abadi et al. 2009; Tissera et al. 2010) leads us to suggest a modified or generalized NFW (GNFW) profile in which the inner total density profile is close to isothermal (with a possible systematic variation with  $M_{\text{vir}}$ ) while the NFW profile is kept at large radii well outside the stellar mass distributions. The GNFW profile is then (in an average sense) preserved in the successive merging of GNFWs. Furthermore, the evolution of the concentration of such an GNFW profile with  $z$  at fixed  $M_{\text{vir}}$  conspires with the evolution of the virial radius  $r_{\text{vir}}$  with  $z$  to lead to a non-varying  $\sigma$  with  $z$ . It is not well understood at present whether this is just a coincidence or a revelation of a fundamental mechanism in galaxy formation and evolution. It is also not clear whether the non-evolving  $M_{\text{vir}}-\sigma$  relation extends to a higher redshift, i.e., since when the HMF and the VDF have been coevolving in parallel in cosmic history.

The observation that the amount of star formation (i.e. stellar mass  $M_{\star}$ ) is correlated with  $M_{\text{vir}}$  (e.g. Conroy & Wechsler 2009; Moster et al. 2009; Guo et al. 2009; Behroozi et al. 2010) is consistent with the above picture. Namely, a larger halo undergoes a larger amount of star formation needed to modify the greater potential well. If  $M_{\star}$  were perfectly correlated with  $\sigma$  at fixed  $M_{\text{vir}}$ , the correlation between  $M_{\text{vir}}$  and  $\sigma$  would be just a by-product of the  $M_{\text{vir}}-M_{\star}$  correlation. However, although there is some good correlation between  $M_{\star}$  and  $\sigma$  for all galaxies (i.e. regardless of their haloes), the correlation between  $M_{\star}$  and  $\sigma$  at fixed  $M_{\text{vir}}$  is weaker (in preparation). Hence, under the above picture the  $M_{\text{vir}}-\sigma$  correlation is originated from the  $\Lambda$ CDM haloes and the amount of star formation set by  $M_{\text{vir}}$  rescales the correlation. We then expect some correlation between  $M_{\star}$  and  $\sigma$  at fixed  $M_{\text{vir}}$  because the boost of  $\sigma$  depends on the degree of the baryonic effects on the halo characterized by  $M_{\star}$  (in preparation).

Let us compare the coevolution and the above picture motivated by it with some pictures (or interpretations) and numerical simulation results of the  $\Lambda$ CDM paradigm that

<sup>5</sup> Given the observational uncertainty of the Spitzer SMF at  $z = 1$  it is only marginally inconsistent with zero evolution (see Behroozi et al. 2010).

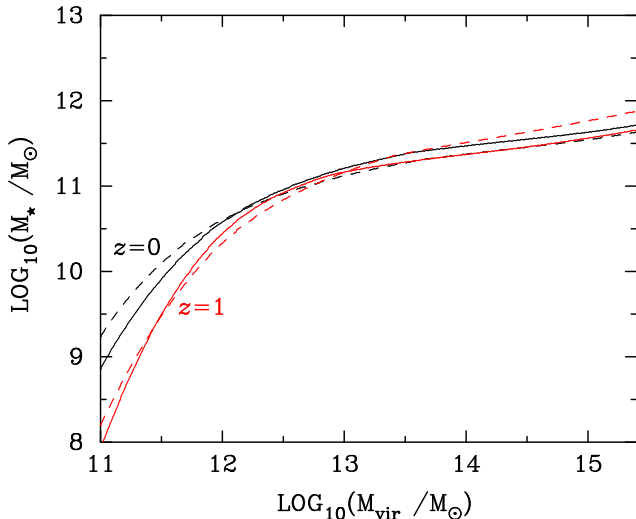


**Figure 9.** The abundance matching relations between  $M_{\text{vir}}$  (halo virial mass) and  $M_{\star}$  (central galaxy stellar mass) at  $z = 0$  (black curves) and  $z = 1$  (red curves) based on the COSMOS (solid curves) and the Spitzer (dashed curves) SMFs. These results are based on a constant intrinsic scatter of 0.16 for  $\log_{10}(M_{\star}/M_{\odot})$  at fixed  $M_{\text{vir}}$ .

have been discussed in the literature. First, the continual growth of the central stellar velocity dispersion and the stellar mass accompanying the growth of the halo over cosmic time would be inconsistent with a strictly “stable core concept” for massive galaxies (e.g. Loeb & Peebles 2003; Gao et al. 2004) even after  $z = 1$ . However, the growth slopes for  $\sigma$  and  $M_{\star}$  are shallower for more massive haloes according to the abundance matching results (see Fig. 4 and Fig. 9). Hence a weakly evolving core of massive haloes would be consistent with our results. Second, the picture shares the concept of “universal density profile” with the attractor hypothesis (e.g. Loeb & Peebles 2003; Gao et al. 2004). However, there is a clear distinction between the two. The attractor hypothesis assumes that the universal NFW profile is preserved or restored in hierarchical merging of haloes (hosting galaxies) while the present picture assumes that the baryon-modified universal total density profile (i.e. the GNFW profile) is preserved once it is created. The latter property is supported by dissipationless merging simulations (e.g. Boylan-Kolchin & Ma 2004; Kazantzidis et al. 2006; Nipoti et al. 2009).

*Test of the  $\Lambda$ CDM paradigm?*: The basic tenet of the  $\Lambda$ CDM structure formation theory is the hierarchical mass assembly. What the theory predicts is the distribution of dark matter haloes. Connecting observed galaxies with theoretical dark haloes is a major goal of cosmological research. The difficulty of testing the  $\Lambda$ CDM paradigm arises from the complex physics of galaxy formation within the halo and the induced modification of the halo structure. A necessary condition for a successful model is to reproduce the basic statistical properties of the observed local Universe, such as the luminosity, stellar mass and velocity functions of galaxies and their correlations (see Trujillo-Gomez et al. 2010). However, a successful reproduction of the  $z = 0$  statistical properties of galaxies is not sufficient. A successful

model must predict correctly the evolution of the galaxy properties. Semi-analytic models of galaxy formation have paid much attention on the galaxy luminosity and stellar mass functions. The current generation of these models can reproduce the  $z = 0$  functions reasonably well, but fail to match their observed evolutions (see, e.g., Fontanot et al. 2009; Stringer et al. 2009; Cattaneo et al. 2008).

The galaxy luminosity and stellar mass functions have much to do with the complex baryonic physics of star formations, AGN activities, feedbacks, etc. Hence the evolutions of the galaxy luminosity and stellar mass functions can only provide indirect tests of the underlying  $\Lambda$ CDM paradigm. The stellar velocity or velocity dispersion of the galaxy residing in the centre of a halo probes the gravitational potential of the baryon plus dark matter system. Since the dark halo is expected to be modified in the course of the dissipational galaxy formation process (e.g. Blumenthal et al. 1986; Gnedin et al. 2004; Rudd et al. 2008; Abadi et al. 2009; Tissera et al. 2010) and the central potential is likely to be dominated by the baryonic matter, the velocity (dispersion) function evolution itself is not a direct probe of the  $\Lambda$ CDM paradigm either. However, the velocity (dispersion) function is separated from much of the baryonic physics but has only to do with its dynamical effect. Hence, once the dynamical effect of galaxy formation is well accounted for, the evolution of the velocity (dispersion) function offers an useful complementary probe of the structure formation theory. While it is challenging to measure reliably the evolution of the velocity (dispersion) function through conventional galaxy surveys, strong lensing statistics in a well-defined survey provides an excellent opportunity to constrain the evolution of the velocity (dispersion) function through the image splitting distributions (see Chae 2010). Current strong lensing statistics is limited by the small sample size. However, future cosmological surveys including (but not limited to) the Dark Energy Survey, the Large Synoptic Survey Telescope and the Square Kilometre Array will increase dramatically the number of strong lenses (see Oguri & Marshall 2010) allowing to put tight constraints on the evolution of velocity (dispersion) functions.

## 6 CONCLUSIONS

Through an abundance matching analysis of the lensing constrained VDF evolution along with the theoretical HMF and the observed SMF from galaxy surveys, we find the following.

- (i) The dark halo virial mass-central stellar velocity dispersion ( $M_{\text{vir}}-\sigma$ ) relation at  $z = 0$  is in excellent agreement with the observed properties of low-redshift individual haloes.
- (ii) The stellar mass-central stellar velocity dispersion ( $M_{\star}-\sigma$ ) relation at  $z = 0$  is consistent with the local scaling relations of galaxies in the literature.
- (iii) The  $M_{\text{vir}}-\sigma$  relation does not evolve between  $z = 1$  and 0 independent of current observation and simulation data.
- (iv) The  $M_{\star}-\sigma$  relation does not evolve between  $z = 1$  and 0 for the COSMOS SMF. This is well in line with the observed non-evolution of  $\sigma$  with  $z$  at  $M_{\star} = 10^{11} M_{\odot}$ . This

is also consistent with the predicted little or mild evolution of  $\sigma$  with  $z$  insensitive to  $M_\star$  from cosmological simulations. However, the Spitzer SMF (a typical downsizing SMF) requires the  $M_\star$ - $\sigma$  relation to evolve in a differential way that is not supported by independent observational results on the structural evolutions of galaxies in the literature.

(v) The non-evolution in the  $M_{\text{vir}}\text{-}\sigma$  and the  $M_\star\text{-}\sigma$  relations imply a parallel coevolution of  $M_{\text{vir}}$ ,  $M_\star$  and  $\sigma$  between  $z = 1$  and 0. This is corroborated by the little evolution in the abundance matching  $M_{\text{vir}}\text{-}M_\star$  relation between  $z = 1$  and 0 for  $M_{\text{vir}} \gtrsim 10^{12} M_\odot$ .

(vi) The parallel coevolution of  $M_{\text{vir}}$ ,  $\sigma$  and  $M_\star$  with  $z$  may imply a universality and regularity in galaxy formation and evolution despite complex baryonic physics processes.

The author would like to thank Mariangela Bernardi, Nacho Trujillo and Michele Cappellari for useful communications and Andrey Kravtsov, Robert Feldmann, Joshua Frieman, Nick Gnedin and Steve Kent for helpful discussions and conversations. The author also gratefully acknowledges the referee comments that were helpful in clarifying and improving the manuscript significantly.

## REFERENCES

- Abadi M. G., Navarro J. F., Fardal M., Babul A., Steinmetz M., 2010, MNRAS, in press (arXiv:0902.2477)
- Auger M. W., Treu T., Bolton A. S., Gavazzi R., Koopmans L. V. E., Marshall P. J., Bundy K., Moustakas L. A., 2009, ApJ, 705, 1099
- Battaglia G., et al., 2005, MNRAS, 364, 433
- Battaglia G., et al., 2006, MNRAS, 370, 1055
- Behroozi P. S., Conroy C., Wechsler R. H., 2010, ApJ, 717, 379
- Bell E. F., et al., 2004, ApJ, 608, 752
- Bell E. F., McIntosh D. H., Katz N., Weinberg M. D., 2003, ApJS, 149, 289
- Bernardi M., Shankar F., Hyde J. B., Mei S., Marulli F., Sheth R. K., 2010, MNRAS, 404, 2087
- Bezanson R., van Dokkum P. G., Tal T., Marchesini D., Kriek M., Franx M., Coppi P., 2009, ApJ, 697, 1290
- Blumenthal G. R., Faber S. M., Flores R., Primack J. R., 1986, ApJ, 301, 27
- Bolton A. S., Treu T., Koopmans L. V. E., Gavazzi R., Moustakas L. A., Burles S., Schlegel D. J., Wayth R., 2008, ApJ, 684, 248
- Bower R. G., Benson A. J., Malbon R., Helly J. C., Frenk C. S., Baugh C. M., Cole S., Lacey C. G., 2006, MNRAS, 370, 645
- Boylan-Kolchin M., Ma C.-P., 2004, MNRAS, 349, 1117
- Brown M. J. I., Zheng Z., White M., Dey A., Jannuzzi B. T., Benson A. J., Brand K., Brodwin M., Croton D. J., 2008, ApJ, 682, 937
- Bryan G. L., Norman M. L., 1998, ApJ, 495, 80
- Bullock J. S., Kolatt T. S., Sigad Y., Somerville R. S., Kravtsov A. V., Klypin A. A., Primack J. R., Dekel A., 2001, MNRAS, 321, 559
- Bundy K., Fukugita M., Ellis R. S., Targett T. A., Belli S., Kodama T., 2009, ApJ, 697, 1369
- Cappellari M., et al., 2006, MNRAS, 366, 1126
- Cappellari M., et al., 2009, ApJ, 704L, 34
- Cattaneo A., Dekel A., Faber S. M., Guiderdoni B., 2008, MNRAS, 389, 567
- Cenarro A. J., Trujillo I., 2009, ApJ, 696L, 43
- Chae K.-H., 2010, MNRAS, 402, 2031
- Chae K.-H., Mao S., Kang X., 2006, MNRAS, 373, 1369
- Chartas G., Gupta V., Garmire G., Jones C., Falco E. E., Shapiro I. I., Tavecchio F., 2002, ApJ, 565, 96
- Choi, Y.-Y., Park, C., & Vogeley, M. S. 2007, ApJ, 658, 884
- Cimatti A., Daddi E., Renzini A., 2006, A&A, 453, L29
- Cimatti A., et al., 2008, A&A, 482, 21
- Conroy C., Wechsler R. H., 2009, ApJ, 696, 620
- Conroy C., Wechsler R. H., Kravtsov A. V. 2006, ApJ, 647, 201
- Conselice C. J., et al., 2007, MNRAS, 381, 962
- Cool R. J., et al., ApJ, 682, 919
- Courteau S., McDonald M., Widrow L. M., Holtzman J., 2007, ApJ, 655L, 21
- de Ravel L., et al., 2009, A&A, 498, 379
- Desroches L.-B., Quataert E., Ma C.-P., West A. A., 2007, MNRAS, 377, 402
- di Serego Alighieri S., et al., 2005, A&A, 442, 125
- Dunkley J., et al., 2009, ApJS, 180, 306
- Dutton A. A., Conroy C., van den Bosch F. C., Prada F., More S., 2010, MNRAS, in press (arXiv:1004.4626)
- Faber S. M., et al., 2007, ApJ, 665, 265
- Feldmann R., Carollo C. M., Mayer L., Renzini A., Lake G., Quinn T., Stinson G. S., Yepes G. 2010, ApJ, 709, 218
- Ferrarese L., 2002, ApJ, 578, 90
- Fontana A., et al., 2006, A&A, 459, 745
- Fontanot F., De Lucia G., Monaco P., Somerville R. S., Santini P., 2009, MNRAS, 397, 1776
- Gao L., Loeb A., Peebles P. J. E., White S. D. M., Jenkins A., 2004, ApJ, 614, 17
- Gavazzi R., et al., 2007, ApJ, 667, 176
- Gnedin O. Y., Kravtsov A. V., Klypin A. A., Nagai D., 2004, ApJ, 616, 16
- Grillo C., Gobat R., Lombardi M., Rosati P., 2009, A&A, 501, 461
- Guo Q., White S., Li C., Boylan-Kolchin M., 2009, MNRAS, submitted (arXiv:0909.4305)
- Ho L. C., 2007, ApJ, 668, 94
- Hopkins P. F., Bundy K., Hernquist L., Wuyts S., Cox T. J., 2010, MNRAS, 401, 1099
- Hopkins P. F., Bundy K., Murray N., Quataert E., Lauer T. R., Ma C.-P., 2009a, MNRAS, 398, 898
- Hopkins P. F., Hernquist L., Cox T. J., Keres D., Wuyts S., 2009b, ApJ, 691, 1424
- Hyde J. B., Bernardi M., 2009, MNRAS, 396, 1171
- Ilbert O., et al., 2010, ApJ, 709, 644
- Jenkins A., Frenk C. S., White S. D. M., Colberg J. M., Cole, S., Evrard A. E., Couchman H. M. P., Yoshida N., 2001, MNRAS, 321, 372
- Kazantzidis S., Zentner A. R., Kravtsov A. V., 2006, ApJ, 641, 647
- Kitzbichler M. G., White S. D. M., 2007, MNRAS, 376, 2
- Klypin A. A., Trujillo-Gomez S., Primack J., 2010, ApJ, submitted (arXiv: 1002.3660v3)
- Klypin A., Zhao H., Somerville R. S., 2002, ApJ, 573, 597
- Kochanek C. S., White M., 2001, ApJ, 559, 531

- Koopmans L. V. E., Treu T., Bolton A. S., Burles S., Moustakas L. A., 2006, ApJ, 649, 599
- Kravtsov A. V., Berlind A. A., Wechsler R. H., Klypin A. A., Gottlöber S., Allgood B., Primack J. R., 2004, ApJ, 609, 35
- Lacey C., Cole S., 1993, MNRAS, 262, 627
- Li L.-X., Ostriker J. P., ApJ, 566, 652
- Loeb A., Peebles P. J. E., 2003, ApJ, 589, 29
- Lokas E. L., Mamon G. A., 2001, MNRAS, 321, 155
- Longhetti M., Saracco P., 2009, MNRAS, 394, 774
- Lukić Z., Heitmann K., Habib S., Bashinsky S., Ricker P. M., 2007, ApJ, 671, 1160
- Macciò A. V., Dutton A. A., van den Bosch F. C., Moore B., Potter D., Stadel J., 2007, MNRAS, 378, 55
- Marchesini D., van Dokkum P. G., Förster S., Natascha M., Franx M., Labbé I., Wuyts S., 2009, ApJ, 701, 1765
- Masjedi M., Hogg D. W., Blanton M. R., 2008, ApJ, 679, 260
- Matsuoka Y., Kawara K., 2010, MNRAS, in press (arXiv:1002.0471)
- Moster B. P., Somerville R. S., Maulbetsch C., van den Bosch F. C., Macciò A. V., Naab T., Oser L., 2009, ApJ, submitted (arXiv:0903.4682)
- Nakajima R., Bernstein G. M., Fadely R., Keeton C. R., Schrabback T., 2009, ApJ, 697, 1793
- Navarro J. F., Hayashi E., Power C., Jenkins A. R., Frenk C. S., White S. D. M., Springel V., Stadel J., Quinn T. R., 2004, MNRAS, 349, 1039
- Navarro J. F., Ludlow A., Springel V., Wang J., Vogelsberger M., White S. D. M., Jenkins A., Frenk C. S., Helmi A., 2010, MNRAS, 402, 21
- Newman A. B., Treu T., Ellis R. S., Sand D. J., Richard J., Marshall P. J., Capak P., Miyazaki S., 2009, ApJ, 706, 1078
- Nipoti C., Treu T., Bolton A. S., 2009, ApJ, 703, 1531
- Oguri M., Marshall P. J., 2010, MNRAS, 405, 2579
- Pérez-González P. G., et al., 2008, ApJ, 675, 234
- Pizagno J., Prada F., Weinberg D. H., Rix H.-W., Pogge R. W., Grebel E. K., Harbeck D., Blanton M., Brinkmann J., Gunn J. E., 2007, AJ, 134, 945
- Pizzella A., Corsini E. M., Dalla Bontà E., Sarzi M., Coccato L., Bertola F., 2005, ApJ, 631, 785
- Pozzetti L., et al., 2007, A&A, 474, 443
- Press W. H., Schechter P., 1974, ApJ, 187, 425
- Reed D. S., Bower R., Frenk C. S., Jenkins A., Theuns T., 2007, MNRAS, 374, 2
- Rudd D. H., Zentner A. R., Kravtsov A. V., 2008, ApJ, 672, 19
- Saha P., Williams L. L. R., Ferreras I., 2007, ApJ, 663, 29
- Scarlata C., et al., 2007, ApJS, 172, 494
- Seigar M. S., Barth A. J., Bullock J. S., 2008, MNRAS, 389, 1911
- Shankar F., Marulli F., Bernardi M., Dai X., Hyde J. B., Sheth R. K., 2010, MNRAS, 403, 117
- Sheth R. K. et al., 2003, ApJ, 594, 225
- Sheth R. K., Tormen G., 1999, MNRAS, 308, 119
- Sheth R. K., Tormen G., 2002, MNRAS, 329, 61
- Springel V., et al., 2005, Nature, 435, 629
- Stringer M. J., Benson A. J., Bundy K., Ellis R. S., Quentin E. L., 2009, MNRAS, 393, 1127
- Tasitsiomi A., Kravtsov A. V., Wechsler R. H., Primack J. R., 2004, ApJ, 614, 533
- Tinker J., Kravtsov A. V., Klypin A., Abazajian K., Warren M., Yepes G., Gottlöber S., Holz D. E., 2008, ApJ, 688, 709
- Tissera P. B., White S. D. M., Pedrosa S., Scannapieco C., 2010, MNRAS, 406, 922
- Tonry J. L., Franx M., 1999, ApJ, 515, 512
- Treu T., Koopmans L. V. E., 2002, ApJ, 575, 87
- Trujillo I., Conselice C. J., Bundy K., Cooper M. C., Eisenhardt P., Ellis R. S., 2007, MNRAS, 382, 109
- Trujillo-Gomez S., Klypin A., Primack J., Romanowsky A. J., 2010, arXiv1005.1289
- Vale A., Ostriker J. P., 2004, MNRAS, 353, 189
- van der Wel A., Franx M., van Dokkum P. G., Rix H.-W., Illingworth G. D., Rosati P., 2005, ApJ, 631, 145
- van der Wel A., Holden B. P., Zirm A. W., Franx M., Retter A., Illingworth G. D., Ford H. C., 2008, ApJ, 688, 48
- van Dokkum P. G., et al., 2008, ApJ, 677L, 5
- van Dokkum P. G., Kriek M., Franx M., 2009, Nature, 460, 717
- Wake D. A., et al., 2008, MNRAS, 387, 1045
- Warren M. S., Abazajian K., Holz D. E., Teodoro L., 2006, ApJ, 646, 881
- Wechsler R. H., Bullock J. S., Primack J. R., Kravtsov A. V., Dekel A., 2002, ApJ, 568, 52
- Winn J. N., Rusin D., Kochanek C. S., 2004, Nature, 427, 613
- White S. D. M., Rees M. J., 1978, MNRAS, 183, 341
- White M., Zheng Z., Brown M. J. I., Dey A., Jannuzzi B. T., 2007, ApJ, 655L, 69
- Xue X. X., et al., 2008, ApJ, 684, 1143

## APPENDIX A: INTRINSIC SCATTERS AND BIAS CORRECTIONS FOR THE ABUNDANCE MATCHING RELATIONS

This work is concerned with the abundance matching (AM) relations between  $\sigma$  and  $M_{\text{vir}}$  and between  $\sigma$  and  $M_*$ . The AM is intended to recover the true median relation. If there were not any intrinsic scatter in the relation between two parameters, the AM by equation (2) of two statistical functions would recover the true relation exactly. In reality the distribution of two observables in a plane has intrinsic scatters around the median relation. When there are such intrinsic scatters, the AM by equation (2) will give a biased median relation that is different from the true median relation. Here we estimate the bias and correct the AM relation by equation (2) to obtain the corrected relation. The bias-corrected AM relation is then checked for self-consistency through a Monte-Carlo simulation. In other words, we estimate the bias so that the corrected relation reproduces from one statistical function to the other through a Monte-Carlo simulation based on the intrinsic scatter.

For our purpose a knowledge of the intrinsic scatter is required. There has been no measurement or simulation for the intrinsic scatter in the  $M_{\text{vir}}-\sigma$  relation. On the other hand, there have been measurements for the relation between  $M_*$  and  $\sigma$  (e.g. Desroches et al. 2007; Hyde & Bernardi 2009; Shankar et al. 2010). Hence we study first the  $M_*-\sigma$  relation using a model intrinsic scatter motivated from observed intrinsic scatters. We then give

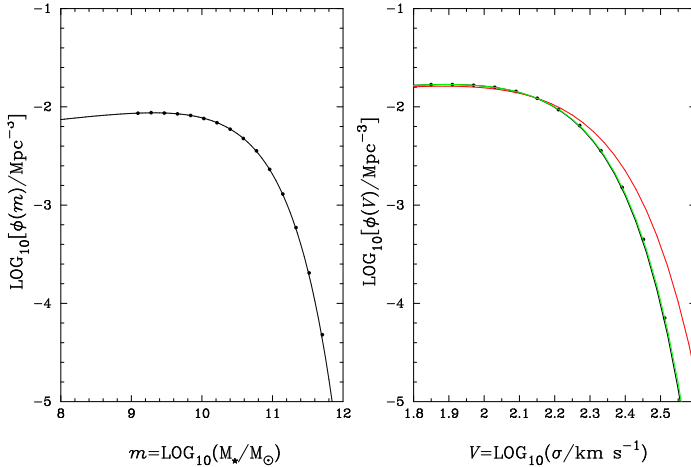


**Figure A1.** Left panel: The SMF for all galaxies measured by Bernardi et al. (2010) based on SDSS DR6 and data points realised by a Monte-Carlo simulation. Right panel: The black curve is the VDF measured by Bernardi et al. (2010) for  $\sigma > 125 \text{ km s}^{-1}$  based on SDSS DR6. The data points and green curve are the results of a Monte-Carlo simulation based on the bias-corrected AM relation and the intrinsic scatter shown in Fig. A2. The red curve is the simulation result based on the biased AM relation shown in Fig. A2.

some results on the  $M_{\text{vir}}-\sigma$  relation that come from a procedure to simultaneously derive an intrinsic scatter and the bias-corrected  $M_{\text{vir}}-\sigma$  relation by considering a bivariate distribution of  $M_*$  and  $\sigma$  as a function of  $M_{\text{vir}}$  (in preparation). Studies on the effects of the intrinsic scatters in the  $M_{\text{vir}}-M_*$  and the  $M_{\text{vir}}-L$  relations can be found respectively in Behroozi et al. (2010) and Tasitsiomi et al. (2004).

For the purpose of demonstration we use the SDSS SMF and VDF by Bernardi et al. (2010) that are displayed in Fig. A1. For the intrinsic scatter of  $V[\equiv \log_{10}(\sigma/\text{km s}^{-1})]$  as a function of  $m[\equiv \log_{10}(M_*/M_\odot)]$ , we adopt a linear model given by  $0.115 - 0.039 \times (m - 10)$  that is derived from the Desroches et al. (2007) measurements of early-type galaxies for  $m \gtrsim 10.4$  and are consistent with the measurements by Hyde & Bernardi (2009) and Shankar et al. (2010). For all galaxies including late-type galaxies, the intrinsic scatter will be more complicated than this. In this work we do not attempt to consider an intrinsic scatter distribution for all galaxies for the following two reasons. First, there have not been any published measurement results of the intrinsic scatter for all galaxies. Second, the intrinsic scatter for early-type galaxies will match that for all galaxies at large stellar masses where the bias in AM is most significant. In other words, we can reliably estimate the greatest bias in AM using only the intrinsic scatter for early-type galaxies.

Fig. A2 shows the biased (red curve) and the bias-corrected (green curve) AM relations. The dashed curves around the bias-corrected AM relation represent the adopted intrinsic scatter described above. Fig. A1 shows the input VDF and the Monte-Carlo simulated VDFs from the input SMF based on the biased and bias-corrected AM relations and the adopted intrinsic scatter. Notice that for the bias-corrected AM relation the simulated VDF closely matches the input VDF. Hence the required self-consistency is gained. If we use different input SMFs and VDFs, we will

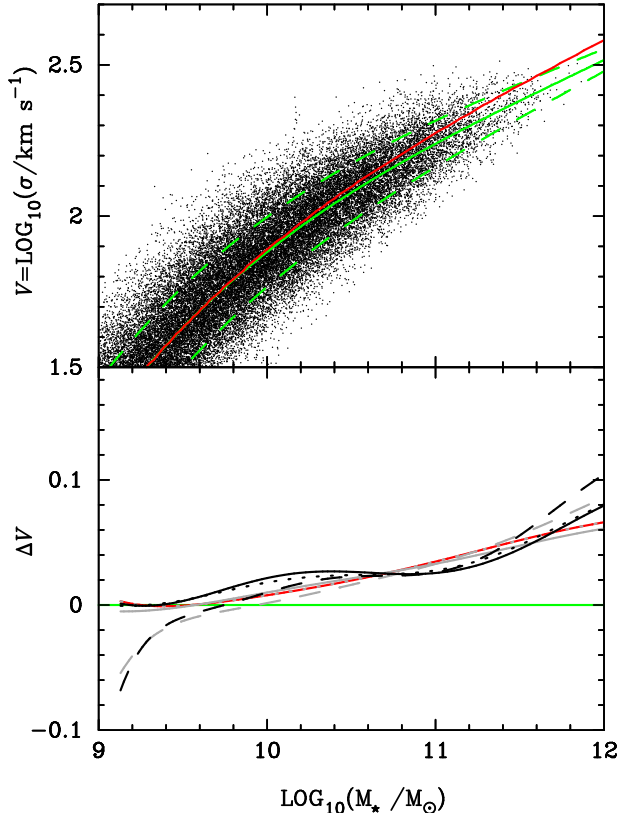


**Figure A2.** Upper panel: Red curve is the AM relation given by equation 2 for the SMF and the VDF shown in Fig. A1 while green curve is an adjusted relation. Green dashed curves represent  $1\sigma$  dispersion assuming a gaussian distribution of  $V[\equiv \log_{10}(\sigma/\text{km s}^{-1})]$ . Data points have been realized from the SMF using the adjusted relation and the adopted scatter. A VDF derived from these simulated data points matches nearly perfectly the input VDF. The adjusted relation is referred to as the bias-corrected relation in the texts. Lower panel: The difference between the initial AM relation (equation 2) and the adjusted relation, referred to as the AM bias. Red curve is that for the upper panel. Other curves are for the following input SMFs and VDFs: (1) black solid - Chae VDF/COSMOS SMF; (2) black dashed - Chae VDF/Spitzer SMF; (3) black dotted - Chae VDF/Bernardi SMF; (4) gray solid - Bernardi VDF/COSMOS SMF; (5) gray dashed - Bernardi VDF/Spitzer SMF; (6) gray dotted - Bernardi VDF/Bernardi SMF (identical to the red curve).

of course get different AM biases. Several biases required for the  $z = 0$  SMFs and VDFs used in this work can be found in the bottom panel of Fig. A2. To estimate the biases required for the  $z = 1$  functions we use the predicted VDFs at  $z = 1$  based on the best-fit evolution parameters from strong lensing statistics along with the observed  $z = 1$  SMFs. The magnitude of the biases for  $z = 1$  is about the same as that for  $z = 0$  and we do not display the  $z = 1$  biases.

The same procedure would be followed for the  $M_{\text{vir}}-\sigma$  relation if there were an observational intrinsic scatter as for the  $M_*$ - $\sigma$  relation above. Without a knowledge of the intrinsic scatter for the  $M_{\text{vir}}-\sigma$  relation we devise a procedure that allows us to derive simultaneously the intrinsic scatter and the median relation for  $M_{\text{vir}}$  and  $\sigma$  (in preparation). A full description of the procedure is beyond the scope of

this paper and the reader is referred to a following paper in preparation. Here we only give a brief description of the procedure and quote a simple result. The idea is to use a bivariate distribution of  $M_*$  and  $\sigma$  at fixed  $M_{\text{vir}}$  noticing that  $M_*$  and  $\sigma$  are expected to be correlated. Then, we determine simultaneously the scatter of  $\sigma$  and the correlation coefficient between  $M_*$  and  $\sigma$  given the observed scatter of  $M_*$  at fixed  $M_{\text{vir}}$  so that the resulting  $M_*$ - $\sigma$  relation is consistent with the given relation based on observations. The results depend on the input scatter of  $M_*$  and the input  $M_*$ - $\sigma$  relation. Fig. 4 shows a simple result based on a standard deviation of 0.16 for  $\log_{10}(M_*)$  at fixed  $M_{\text{vir}}$  and the above described  $M_*$ - $\sigma$  relation based on the Bernardi et al. (2010) observational results.

## APPENDIX B: THE $v_{\text{vir}}\text{-}v_{\text{opt}}$ RELATION AT $Z = 0$

Dutton et al. (2010) constrain the relation between  $v_{\text{vir}}$  and  $v_{\text{opt}}$  through combining observationally derived  $M_*$ - $M_{\text{vir}}$  and  $M_*$ - $v_{\text{opt}}$  relations ( $v_{\text{vir}}$  and  $v_{\text{opt}}$  are the circular rotation velocities at the virial and the optical radii respectively). The abundance matching  $M_{\text{vir}}\text{-}\sigma$  relation from this work may be transformed into a  $v_{\text{vir}}\text{-}v_{\text{opt}}$  relation using an empirical relation between  $v_{\text{opt}}$  and  $\sigma$ . The virial velocity  $v_{\text{vir}}$  is defined by  $\sqrt{GM_{\text{vir}}/r_{\text{vir}}}$  where the virial radius at  $z = 0$  is given by (Bryan & Norman 1998)

$$r_{\text{vir}} \approx 209h^{-1} \left( \frac{M_{\text{vir}}}{10^{12}h^{-1}\text{M}_\odot} \right)^{1/3} \text{kpc} \quad (\text{B1})$$

for the adopted cosmology and we take  $h = 0.7$ .

For early-type (elliptical and lenticular) galaxies, the direct estimate of  $v_{\text{opt}}/\sigma$  ranges from  $\approx \sqrt{2}$  to  $\approx 1.7$  (e.g. Courteau et al. 2007; Ho 2007; Pizzella et al. 2005; Ferrarese 2002). For late-type galaxies the Chae (2010) late-type VDF has actually been transformed from a circular velocity function (VF) assuming  $v_{\text{opt}}/\sigma = \sqrt{2}$ . Hence we can transform the Chae (2010) late-type VDF back to the original VF using the same factor. The Bernardi et al. (2010) VDF is a directly measured function based on SDSS spectroscopy. It is important to note that the SDSS measured velocity dispersions for late-type galaxies with small bulges (or without bulges) come mostly from rotational motions (M. Bernardi, private communications), meaning that these small-bulge (bulge-less) systems are not missed in the Bernardi et al. (2010) VDF. Hence we need an independent knowledge of  $v_{\text{opt}}/\sigma$  for SDSS galaxies to transform the Bernardi et al. (2010) VDF to a VF. Without a measured value of  $v_{\text{opt}}/\sigma$  for SDSS galaxies we must resort to other measurements. From the literature we find  $v_{\text{opt}}/\sigma \approx 1.4 - 2$  for late-type galaxies depending on the bulge-to-disk ratio (e.g. Courteau et al. 2007; Ho 2007; Pizzella et al. 2005; Ferrarese 2002).

Based on these literature values of  $v_{\text{opt}}/\sigma$  for early- and late-type galaxies we adopt a range of  $v_{\text{opt}}/\sigma = \sqrt{2} - 1.7$  independent of galaxy type to estimate the circular velocity function of galaxies and then the  $v_{\text{vir}}\text{-}v_{\text{opt}}$  relation through abundance matching. Fig. B1 shows the likely range of the median value for  $v_{\text{opt}}/v_{\text{vir}}$  as a function of  $v_{\text{vir}}$ . Compared with Fig. 5 of Dutton et al. (2010) our results for massive galaxies ( $v_{\text{vir}} \gtrsim 10^{2.3} \approx 200 \text{ km s}^{-1}$ ) overlap with the Dutton et al. (2010) results for early-type galaxies. For

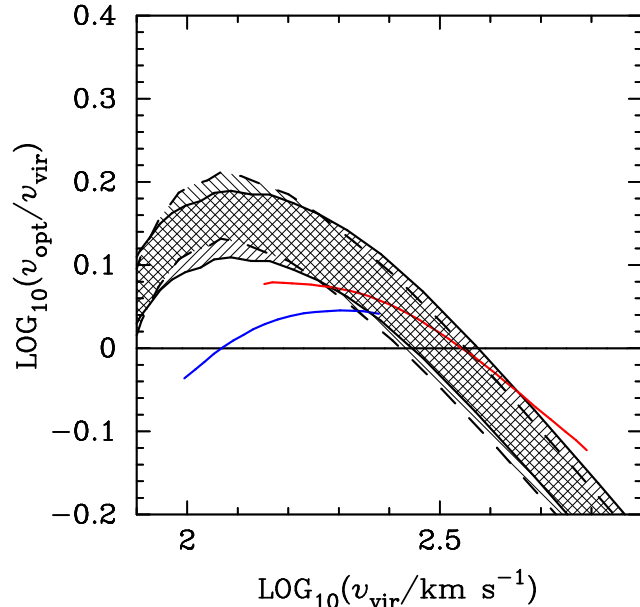


**Figure B1.** The relation between the halo circular velocity at the virial radius ( $v_{\text{vir}}$ ) and the stellar circular velocity in the optical region ( $v_{\text{opt}}$ ) of the central galaxy at  $z = 0$ , inferred from the abundance matching relation between  $M_{\text{vir}}$  (halo virial mass) and  $\sigma$  (central stellar velocity dispersion) from the VDF and the  $\Lambda\text{CDM}$  halo mass function (see the texts in §3.2). The solid and dashed curves are respectively based on the VDFs by Chae (2010) and Bernardi et al. (2010). For each set of the results the lower and upper curves are respectively based on  $v_{\text{opt}} = \sqrt{2}\sigma$  and  $v_{\text{opt}} = 1.7\sigma$ .

$v_{\text{vir}} \gtrsim 10^{2.3} \text{ km s}^{-1}$  our results give a scaling of  $v_{\text{opt}} \propto v_{\text{vir}}^\gamma$  with  $\gamma \approx 0.3 - 0.4$ . This scaling is consistent with previous results for massive galaxies based on strong lensing statistics and other methods (see Chae et al. 2006 and references therein).

However, our results for less massive galaxies ( $v_{\text{vir}} \lesssim 10^{2.3} \text{ km s}^{-1}$ ) give systematically higher median values of  $v_{\text{opt}}/v_{\text{vir}}$  compared with the Dutton et al. (2010) results for late-type galaxies although the estimated intrinsic scatters (not shown here) overlap. Our results are consistent with declining rotation curves near the virial radii for late-type galaxies while the Dutton et al. (2010) results imply flat rotation curves right up to the virial radii. The possible discrepancy may imply some unidentified systematic errors in one or both of the results. For our results the possible sources of systematic errors include the adopted VDFs and the adopted relation between  $\sigma$  and  $v_{\text{opt}}$ . In order to be consistent with the Dutton et al. (2010) results the number densities of galaxies would have to be significantly lower at relatively low velocity dispersions. We use two independently determined VDFs (i.e. the Chae 2010 and Bernardi et al. 2010 VDFs) and they give similar results for  $v_{\text{opt}}/v_{\text{vir}}$ . In fact, the adopted Bernardi et al. (2010) VDF is the modified Schechter fit result for  $\sigma > 125 \text{ km s}^{-1}$ . This VDF gives an underestimate of galaxy number densities at low  $\sigma$  according to Bernardi et al. (2010) data. Hence if we were using the raw galaxy number densities, the discrepancy with the Dutton et al. (2010) results would get worse at low  $\sigma$ . The adopted range  $v_{\text{opt}}/\sigma = \sqrt{2} - 1.7$  is suggested

by a broad range of observations. A possible cause of error may be that bulgeless late-type galaxies have  $v_{\text{opt}}/\sigma > 1.7$  so that we need to adjust the overall value higher. However, if we adopted  $v_{\text{opt}}/\sigma > 1.7$ , the discrepancy with the Dutton et al. (2010) results would get worse.